EXPERIMENTAL INVESTIGATION OF FRICTIONAL PRESSURE DROP IN INCLINED TUBES

Adelaja A.O.*, Dirker J.** and Meyer J.P***.
*Author for correspondence
Department of Mechanical and Aeronautical Engineering,
University of Pretoria,
Pretoria, 0002,
South Africa,
E-mail: * adekunle.adelaja@up.ac.za ** jaco.dirker@up.ac.za ***josua.meyer@up.ac.za

ABSTRACT

The present paper reports on the two-phase frictional pressure drop calculated during the condensation of R134a in a tube of inner diameter of 8.38 mm at different inclination angles. The pressure drops were calculated using the most recent void fraction model of Bhagwat and Ghajar. The condensation tests were carried out in an experimental test facility with a 1.704 m distance between the differential pressure taps. The operating conditions were for mass fluxes of 200 kg/m^{2}s and 300 kg/m^{2}s, mean vapour qualities between 0.25 and 0.75, a saturation temperature of 40°C and for inclination angles ranging between -90° (downward flow) and +90° (upward flow). The highest values of the void fractions and frictional pressure drops were obtained during the vertical downward flow while the lowest were obtained during the vertical upward flow.

INTRODUCTION

In the design and optimization of heat exchangers such as found in refrigeration, petroleum industries, processing, nuclear and thermal power plants, the knowledge of pressure drops characteristics is paramount. With attention given to inclined tube heat exchangers as in the case of A-frame and V-frame condensers, it is important to understand and predict the relevant pressure drop values. Because data obtained for horizontal and vertical tubes might be insufficient to explain the phenomenon in inclined tubes, studies which specifically focus on the tube orientation are vital.

So far, limited studies have been carried out on two-phase flow frictional pressure drop in inclined tubes. Lips and Meyer [1] investigated the two-phase flow in pressure drops in inclined tubes. The results of the horizontal and vertical cases were compared with some models in literature. A theoretical analysis of the void fraction was conducted and an apparent void fraction was calculated from the apparent gravitational pressure drop at a saturation temperature of 40°C. Adelaja *et al* [2] studied the pressure drop and friction factor in inclined tubes at saturation temperatures of 30°C to 50°C. Results obtained show that the mean vapour quality, mass flux, saturation temperature and inclination angle strongly influences the static and measured pressure drops, but not the momentum pressure drop.

The relation, however, was not extended to the frictional pressure drop. In this study, the frictional pressure drop was investigated using the void fraction of Bhagwat and Ghajar [3] which was formulated for different conditions (including inclined tubes).

NOMENCLATURE

C		Multiplication factors
C_o	[-]	Distribution parameter
d_i	[m]	Tube inner diameter
f_{tp}	[-]	Fanning friction factor based on Re_{tp}
g	[ms^{-2}]	Acceleration due to gravity
G	[kgm^{2}s]	Mass flux
$L_{\Delta P}$	[m]	Distance between pressure taps
P	[Nm^{-2}]	Pressure
x	[-]	Quality
Re_{tp}	[-]	Two-phase Reynolds number
U_m	[ms^{-1}]	Two-phase mixture velocity
U_{gm}	[ms^{-1}]	Drift velocity
U_{sg}	[ms^{-1}]	Vapour phase superficial velocity
U_{sl}	[ms^{-1}]	Liquid phase superficial velocity

Special characters

β	[-]	Inclination angle
Δ	[-]	Differential
ε	[-]	Void fraction
ρ	[kgm^{-3}]	Density

Subscripts

fric	Friction
in	Inlet
l	Liquid
line	Line
m	Mean
meas	Measured
mom	Momentum
out	Outlet
stat	Static/ gravitational
test	Test
tp	Two-phase
v	Vapour

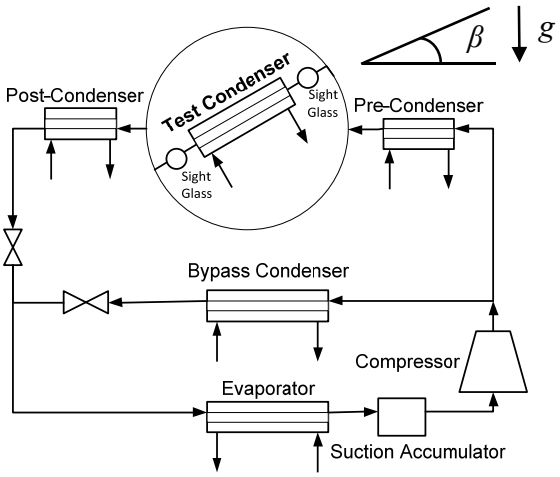

Figure 1 Schematic diagram of the test rig.

EXPERIMENTAL FACILITY

The present study was conducted on an experimental apparatus and set-up in the laboratories of the Department of Mechanical and Aeronautical Engineering, University of Pretoria, South Africa (Figure 1).

The test set-up allowed for double tube condensation heat transfer and pressure drop data to be collected over a wide range of operating conditions. The setup comprised three flow loops: the refrigerant, the cooling water and the hot water loops. In the refrigerant loop, there were two high-pressure lines. The first line contained the pre, test and post condensers, while the second line contained the bypass condenser which was employed to assist in regulating the amount of refrigerant flow through the test condenser.

In the test line superheated vapour from the 10 kW hermetically sealed scroll compressor entered the pre-condenser and was partially condensed to preselected vapour quality depending on the test requirements. The quality achieved at the outlet of the pre-condenser was equal to the inlet quality to the test condenser because the connection interface between the two condensers was adiabatic. The refrigerant entered the test condenser, which carried the refrigerant in an inner tube and water in annulus in a counter flow arrangement, at a prescribed mass and inlet quality. Here, the refrigerant vapour further condensed in the test tube at a prescribed heat flux as controlled via the local cold water flow rate. The heat transfer rate was carefully controlled. The higher the heat transfer rate, the higher the vapour quality difference was between the inlet and the outlet of the test condenser. More information on the test condenser is supplied in the next section. The partially condensed liquid-vapour mixture left the test condenser and was fully condensed in the post-condenser. The post condenser ensured that the two-phase mixture became fully liquid before reaching the electronic expansion valve (EEV). Liquid refrigerant from the two high-pressure lines were combined and flowed to the evaporator where warm water from the hot water flow loop was used to evaporate the liquid refrigerant before the vapour passed to the compressor via the accumulator. All heat exchangers (including all condensers as well as the evaporator) where of the double pipe kind and were operated in counter flow arrangements with the refrigerant flowing in the inner tube and water flowing in the outer annular space. All water and refrigerant flow rates were measured by Coriolis flow meters.

For the water loops, a 50 kW cooling and 70 kW heating dual function heat pump supplied cold and hot water via a distribution system. The cold and hot water temperatures were thermostatically controlled to be 25°C, and 40°C respectively depending on the test conditions. Thermal buffering was obtained by using two 5000 litre insulated water reservoirs to store the hot and cold water.

TEST SECTION

The test condenser was a 1.488 m long counter flow double pipe heat exchanger using water as a coolant in the annulus. The refrigerant vapour condensed inside the inner copper tube. The inner tube had an inner diameter of d_i = 8.38 mm and an outer diameter of 9.55 mm while the annulus had an outer diameter of 15.9 mm. The connections to the test condenser were made of flexible pressure hoses which enabled the test section to rotate according to the inclination angle condition under consideration. To ensure that the flow through the test section was fully developed, a straight calming section, 50 diameters long was situated at the entrance.

All temperature measurements were done with T-type thermocouples calibrated against a high precision Pt-100 resistant temperature. On the test condenser, thermocouples were arranged such that the tube wall temperature could be measured. At each wall measuring location four thermocouples were installed 90° to each other around the tube (i.e. top, bottom and two sides). Twenty-eight of these thermocouples were installed in small pot holes drilled at seven equal-distant positions on the inner tube of the test section. The wall temperatures were used to calculate the heat transfer coefficients, which are not discussed in this paper.

The test section had two pressure ports, one each at the inlet and outlet of the test-tube. The effective pressure drop distance between the ports was $L_{\Delta P}$ = 1.704 m. The pressure drop across the test section was measured by a differential pressure transducer, which was calibrated to an accuracy of ±0.05 kPa. Electrical power was supplied through four heating wires and wrapped around the pressure line between the pressure taps. The heating wires heated the lines such that the temperature was kept at about 5°C to 10°C above the saturation temperature so that condensation was prevented in the line.

At the inlet and outlet of the test section were two sight glasses which enabled flow visualization and also served as insulators against axial heat conduction. A high speed camera was installed at the outlet sight glass and was used to record and document the flow pattern. A uniform Phlox backlight was positioned against the sight glass to enable good colour fidelity due to its evenly distributed light emitting diode (LED) illumination.

EXPERIMENTAL PROCEDURE AND DATA REDUCTION

A large range of experimental conditions were covered during experimental tests. Only a portion of the dataset is covered here. The conditions for the data points under consideration in this paper are presented in Table 1. The mean vapour quality, x_m, is based on the arithmetic average between the entrance and exit qualities of the R134a as obtained by using the energy balance principle for the pre-condenser and test-condenser. After steady state conditions were reached, the different sensor signals were recorded continuously through a Labview and National Instrument data acquisition system for about a period of 10 minutes. Time averaged data was used to minimise the effects of data-noise.

Frictional Pressure Drop

Since frictional pressure drop is an important engineering quantity, a method is needed to obtain this from the overall pressure difference measurements across the test-sections. The recorded pressure difference data, ΔP_{meas}, as obtained by the differential pressure transducer, contained the pressure difference across the test section, ΔP_{test}, as well as the static pressure difference in the pressure lines running between the transducer and the pressure ports, ΔP_{line}. Because different test section inclination angles were considered, the pressure differences inside the pressure lines have to be removed from the measured values:

$$\Delta P_{meas} = \Delta P_{test} + \Delta P_{line} \tag{1}$$

The line pressure difference can be expressed as:

$$\Delta P_{line} = \rho_v g L_{\Delta P} \sin\beta \tag{2}$$

where ρ_v is the density of the vapour in the measuring lines, g is the acceleration due to gravity, $L_{\Delta P}$ is the distance between the pressure taps and β is the angle of inclination of the test section. As mentioned, the pressure lines were heated to ensure that only vapour was present between the pressure ports and the differential pressure transducer. The inclination angle can change sign depending on the direction of flow (upwards or downwards). It is positive during upward flow, zero for horizontal, and negative during downward flow.

The pressure drop in the test section during the condensation process is a function of the kinetic energy of the fluid, the potential energy of the fluid and the frictional interaction between the fluid and the walls of the tube. The kinetic energy effect is represented by the momentum pressure drop, ΔP_{mom}, the potential energy effect is represented by the static pressure drop, ΔP_{stat}, and the interaction between the fluid and the walls of the tube is represented by the frictional pressure drop ΔP_{fric}. Therelation between these can be represented mathematically as:

$$\Delta P_{\text{test}} = \Delta P_{\text{mom}} + \Delta P_{\text{stat}} + \Delta P_{\text{fric}} \tag{3}$$

By obtaining the values of the momentum and static pressure differences, the frictional pressure can be obtained from the experimental measurements. If a homogeneous two-phase flow scenario is assumed, it can be shown that the static pressure drop is dependent on the inclination angle and thus can be expressed as:

$$\Delta P_{stat} = \rho_{tp} g L_{\Delta P} \sin\beta \tag{4}$$

The static pressure difference reduces to zero for horizontally aligned tubes. The two-phase density, ρ_{tp}, of the fluid can be written as a function of the liquid and vapour phase densities, respectively $\rho_l$and ρ_v, and the void fraction, ε, as:

$$\rho_{tp} = \rho_l(1-\varepsilon) + \rho_v\varepsilon \tag{5}$$

The momentum pressure difference is a function of the kinetic energy (in terms of the mass flux) and is also dependent on thermodynamic state and void fraction of the fluid at the entrance and exit of the test tube. This pressure difference and can be written mathematically as:

$$\Delta P_{mom} = G^2\left[\left(\frac{(1-x)^2}{\rho_l(1-\varepsilon)} + \frac{x^2}{\rho_v\varepsilon}\right)_{out} - \left(\frac{(1-x)^2}{\rho_l(1-\varepsilon)} + \frac{x^2}{\rho_v\varepsilon}\right)_{in}\right] \tag{6}$$

Table 1 Experimental parameter ranges.

Parameter	Range / Value	Band
T_{sat}[°C]	40	± 0.6
G [kg/m^{2}s]	200 and 300	± 5
x_m	0.25, 0.5, 0.75	± 0.01
β [°]	-90° to +90°	± 0.1
Q_{H2O} [W]	250	± 20
ΔP [kPa]	-2 to +12	±0.05

Void Fraction Model

The void fraction is an important parameter which is needed to determine the static and momentum pressure differences in the test section. With the void fraction, other values such as the two-phase mixture viscosity, density and actual velocities can be obtained. Several experimental investigations have been conducted to measure the void fraction for various flow pattern regimes and fluids. Also, several models have been developed to correlate the void fraction to measureable quantities such as the phase temperatures and the dimensions of the flow passage. Most correlations are, however, for horizontal and vertical tube orientations with only a limited number of studies focusing on inclined systems [4-8]. The available models can be categorized into three types: slip models; *k-α* models and drift flux model. For this study, the recent Bhagwat and Ghajar drift flux model [3], suitable for inclined passages is used to predict the void fraction in the test section.

According to this modelling approach, the void fraction can be expressed as presented in equation (7) and is dependent on the flow pattern.

$$\varepsilon = \frac{U_{sg}}{C_0\left(U_m + U_{gm}\right)} \tag{7}$$

Here the two phase mixture velocity, U_m, is equal to the summation of the superficial liquid, U_{sl}, and gas, U_{sg}, phase velocities, C_o is the distribution parameter and U_{gm} is the drift velocity. Detailed information on the void fraction correlation can be obtained from reference [3], however, a brief overview is presented here to indicate how the void fractions were obtained in this study.

The distribution parameter, C_o, can be expressed with equation (8) as a function of, among other, the void fraction, inclination angle, and the two-phase Reynolds number Re_{tp}. The Reynolds number is based on the mixed phase velocity and the saturated liquid properties. C_o accounts for the distribution of the gas phase across the pipe cross sectional area and serves as correction factor to the homogenous flow theory.

$$C_o = \frac{2-(\rho_v/\rho_l)^2}{1+(\mathrm{Re}_{tp}/1000)^2} + \frac{\left[\left(\sqrt{\frac{(1+(\rho_v/\rho_l)^2\cos\beta)}{1+\cos\beta}}\right)^{1-\varepsilon}\right]^{2/5} + C_{o,1}}{1+(1000/\mathrm{Re}_{tp})^2} \quad (8)$$

For a circular tube, $C_{o,1}$ is expressed in terms of the relevant velocities, density values, quality and the Fanning friction factor, f_{tp}, as:

$$C_{o,1} = 0.2\left(1-\sqrt{\rho_v/\rho_l}\right)\left[\left(2.6-\frac{U_{sg}}{U_m}\right)^{0.15} - \sqrt{f_{tp}}\right](1-x)^{1.5} \quad (9)$$

The drift velocity is a function of the pipe diameter, pipe inclination, fluid properties and void fraction as are represented in equation (10). It is a measure of the propagation of velocity of gas bubbles in continuous liquid phase. This results from the interaction between gravitational, buoyancy, surface tension and inertial forces. It can be expressed as:

$$U_{gm} = (0.35\sin\beta + 0.45\cos\beta)\sqrt{\frac{gd_i(\rho_l-\rho_v)}{\rho_l}}(1-\varepsilon)^{0.5}C_2C_3C_4 \quad (10)$$

Here C_2 is a function of the liquid phase viscosity, C_3 is a function based on a Laplace variable, and C_4 is based on the inclination angle and the Froude number is based on the superficial gas velocity. Equations (7) to (10) are solved iteratively until a converged void fraction value is obtained.

EXPERIMENTAL RESULTS

Flow Patterns

The two-phase flow pattern is the distribution of the liquid and gas phases in the tube or channel. The patterns have their peculiar flow features as a result of the interplay of shear, gravitational and tension forces between the liquid and gas. The flow pattern influences the heat transfer coefficient and pressure drop and is thus very important in the design of heat exchangers.

For this study, five flow patterns were identified. They were stratified-wavy, annular-wavy, annular, intermittent, and churn flows. This classification is based on that of Kim and Ghajar [9]. Churn flow encompasses the bubbly/slug and annular/ bubbly / slug. Intermittent flow incorporates slug, plug and elongated bubble flows [10]. Stratified-wavy (Figure 2a) ensues during slightly downward orientation. Liquid is mostly located at the bottom of the tube and there are waves at the liquid-vapour interface. For annular-wavy flow (Figure 2b), increase in the velocity of the vapour causes more condensate to accumulate at the top of the tube. Figure 2c shows the annular flow which occurs as a result of high vapour velocity so that the liquid is located uniformly or near uniformly at the perimeter of the tube. During intermittent flow (Figure 2d), the waves at the bottom of the tube are able to reach the top. It also occurs when vapour velocity is so low that vapour is trapped in the liquid. Figure 2e shows churn flow, which occurs mainly during or near vertical orientations (either upward or downward) for low velocity liquid flow. It is the result of slugs of liquid collapsing into the centre of the vapour.

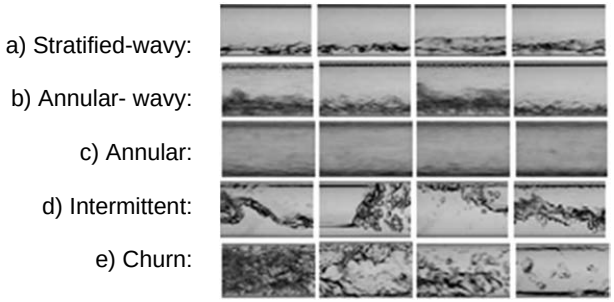

Figure 2 The flow patterns observed during the study.

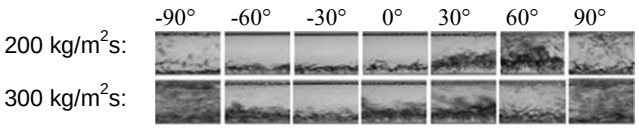

Figure 3 Inclination effect on flow pattern for different G for T_{sat}= 40°C and x_m = 0.5.

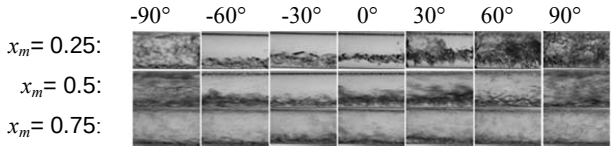

Figure 4 Inclination effect on flow pattern for different x_m for T_{sat} = 40°C and G = 300 kg/m^{2}s.

Figure 3 shows the effect of inclination angle and mass flux on the flow pattern for x_m = 0.5 and T_{sat} = 40°C. The results reveal that as mass flux increases, the flow changes from stratified-wavy, intermittent and churn (at vertical tube orientations) to annular-wavy and churn due to increased shear force. Figure 4 reveals the effect of inclination angle for $0.25 \leq x_m \leq 0.75$, G = 200 kg/m^{2}s and T_{sat} = 40°C. It is shown that x_m and β greatly influence the flow pattern. With an increase in x_m, the flow tends to become annular due to the predomination of the shear force.

Void Fractions

Figure 5 show the effect of inclination angle on the calculated void fraction from eq. (7) for different mean vapour qualities. The void fractions presented here are based on the average vapour quality, and not on the average of the void fraction between the inlet and outlet of the test section. As a general overview, the results show that the void fraction increases with mean vapour qualities. Compared to the effect of the vapour quality, the void fraction was found to be only slightly dependent on the inclination of the tube. The highest void fraction was obtained at β = -90° for all three vapour qualities represented here. This can be explained from the fact that during the downward flow, the action of the gravitational force causes the liquid film on the wall to be thinner hence increased void fraction. The reverse took place during the upward flow.

The effect of mass fluxes as a function of void fraction is revealed in Figure 6. The results show that void fraction is higher with higher mass fluxes. Once again, the highest void fraction was obtained for vertical downward flow, while the lowest was obtained for vertical upward flow. The vertical scatter that is visible in terms of the predicted void fractions is due to the small variations in actual mean vapor quality from one data-point to the next within experimental dataset. It was difficult to maintain the same quality for all test cases, but was within the band reported in Table 1.

Frictional Pressure Drop

The frictional pressure drop is obtained from rearranging equation (3). Figures 7 reveal the variation of the frictional pressure drop with inclination angle for different mean vapour qualities at a saturation temperature of 40°C and a mass flux of 300 kg/m^{2}s. It can be seen that all frictional pressure differences were positive indicating that the there was a drop in pressure associated with the frictional interaction with the tube surface. It can also be seen that the vapour quality had a significant effect of the frictional pressure drop and that higher vapour qualities resulted in higher frictional effects.

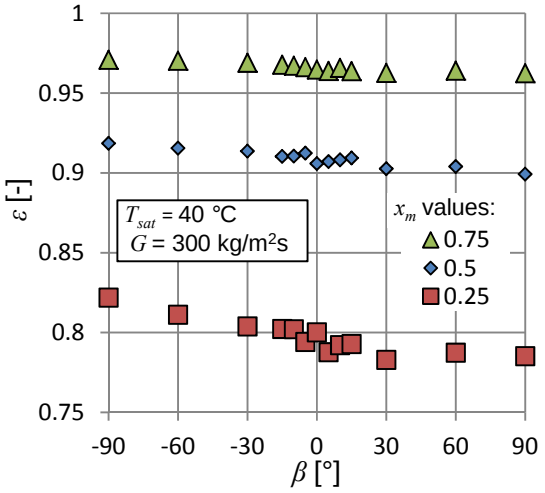

Figure 5 Effect of inclination angle on void fraction at different x_m for G = 300 kg/m^{2}s and T_{sat} = 40°C.

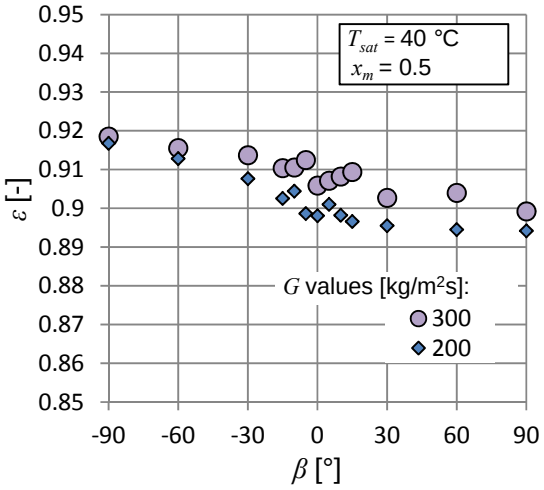

Figure 6 Effect of inclination angle on void fraction at different G for x_m = 0.5 and T_{sat} = 40°C.

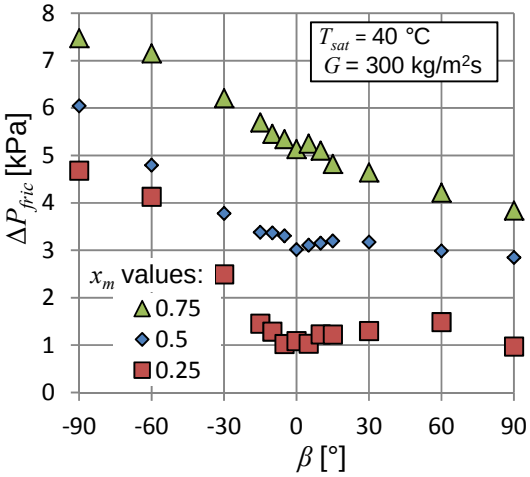

Figure 7 Effect of inclination angle on ΔP_{fric} at different x_m for G = 300 kg/m^{2}s and T_{sat} = 40°C.

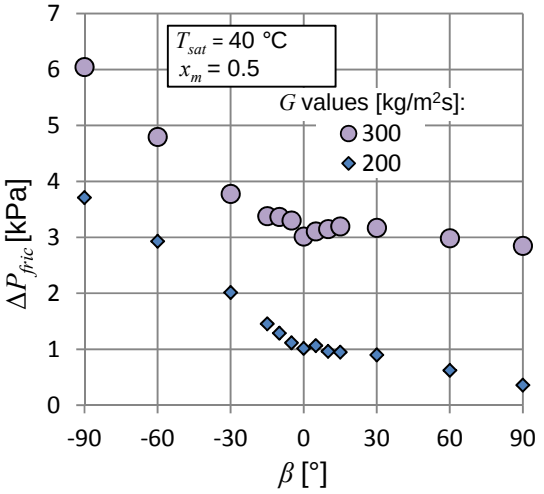

Figure 8 Effect of inclination angle on ΔP_{fric} at different G for x_m = 0.5 and T_{sat} = 40°C.

The highest frictional pressure drop occurred at vertical downward flow, while the lowest frictional pressured drop was generally achieved during upward flow orientations. For vapour qualities of 0.25 and 0.5 there is a hint of a local minimum at $\beta = 0°$ (horizontal flow), but not for a vapour quality of 0.75. In Figure 8 the effect of the mass flux on the frictional pressure drop is shown. It can be seen that the frictional pressure drop increased significantly from 200 kg/m^{2}s to 300 kg/m^{2}s. For both mass flux cases, the highest frictional pressure drop was obtained for vertical downward flow, while the upward flow in general resulted in lower frictional pressure drops. The frictional pressure drop variation can be correlated to the governing flow pattern. Based on the flow patterns presented in Figures 2 and 3 and the frictional pressure difference in Figures 7 and 8, it appears as if stratified, and annular flow patterns were associated with the higher frictional pressure drop.

CONCLUSIONS

In this study, the frictional pressure drop was investigated in inclined tubes using the void fraction model of Bhagwat and Ghajar [3]. The operating conditions that where considered are as follows: inclination angles between -90°(downward flow) and +90° (upward flow), mean vapour qualities of 0.25, 0.5 and 0.75, and mass fluxes of 200 kg/m^{2}s and 300 kg/m^{2}s and a saturation temperature of 40°C. Since the frictional pressure drop is a function of the void fraction, the operating conditions are investigated on both. Results show that both the void fraction and the pressure drop are influenced by these variables. The highest void fraction was obtained during the downward flow while the lowest value is obtained when the tube was inclined upwards. The lowest frictional pressure drop was obtained during the upward tube orientation while the highest values were obtained during downward flows.

REFERENCES

[1] Lips, S. and Meyer, P.J., Experimental study of convective condensation in an inclined smooth tube. Part II: inclination effect on pressure drops and void fractions, *International Journal of Heat and Mass Transfer,* Vol. 55, 2012, pp. 405-412.

[2] Adelaja, A.O., Dirker, J., Meyer, J.P., "Experimental investigation on pressure drop and friction factor in tubes at different inclination angles during the condensation of R134a, *Proceedings of the 15th International Heat Transfer Conference, (IHTC-15),* Kyoto, 2014, pp. 1- 14.

[3] Bhagwat, S.M. and Ghajar, A. J., A flow pattern independent drift flow model based void fraction correlation for a wide range of gas-liquid two-phase flow, *International Journal of Multiphase Flow,* Vol. 59, 2014, pp. 188-205.

[4] Ghajar, A.J and Bhagwat, S.M., Effect of void fraction and two-phase dynamic viscosity models on prediction of hydrostatic and frictional pressure drop in vertical upward gas-liquid two-phase flow, *Heat Transfer Engineering*, Vol. 34, 2013, pp 1044-1059.

[5] Ghajar, A.J and Tang, C.C., Void fraction and flow pattern of two phase flow in upward, downward and horizontal pipes, *Advanced Multiphase Flow Heat Transfer*, Chapter 4, 2012, pp 175-201.

[6] Kaji, M and Azzopardi, B. J., The effect of pipe diameter on the structure of gas-liquid flow in vertical pipes, *International Journal of Multiphase Flow*, Vol. 36, 2010, pp. 303 – 313.

[7] Mishima, K and Hibiki, T., Some characteristics of air-water in two phase flow in small diameter vertical tubes, *International Journal of Multiphase Flow*, Vo. 22, 1996, pp. 703-712.

[8] Shoukri, M., Hassan, I and Gerges, I., Two-phase bubbly floe structure in large diameter vertical pipe, *The Canadian Journal of Chemical Engineering*, Vol. 81, 2003, 205-211.

[9] Kim, D.,Ghajar, A.J., Heat transfer measurement and correlations for air-water flow of different flow patterns in a horizontal pipe, *Experimental Thermal Fluid Science*, Vol. 25, 2002,pp. 659 - 676.

[10] Kokal, S.L.,Stanislav, J.F., An experimental study of two-phase in slightly inclined pipes – 1. Flow pattern, *Chemical Engineering Science*, Vol. 44,Issue 3, 1989,pp. 665 - 679.

FLOW REGIME OF DOWNWARD AIR-WATER TWO-PHASE FLOW IN A VERTICAL NARROW RECTANGULAR CHANNEL

T.H. Kim, B.J. Yun and J.H. Jeong*
*Author for correspondence
School of Mechanical Engineering,
Pusan National University,
Geumjeong-gu, Busan, Korea.
E-mail: jihwan@pusan.ac.kr

ABSTRACT

Downward air-water two-phase flow in vertical rectangular channel was experimentally observed. The depth, width, and length of the rectangular channel is 2.35 mm, 66.7 mm, and 780 mm, respectively. The test section consists of transparent acrylic plates confined within a stainless steel frame. The flow patterns of the downward flow in high liquid velocity appeared to be similar to those observed in previous studies with upward flow. In downward flow, the transition lines for bubbly-slug and slug-churn flow shift to left in the flow regime map constructed with abscissa of the superficial gas velocity and ordinate of the superficial liquid velocity. The flow patterns observed with downward flow at low liquid velocity are different from those with upward flow. Bubbles grow much larger than channel depth at very low liquid and gas flow velocities. The large bubbles would not move upward or downward but stay in the middle of the test section for a long time. The flow regime transitions in high liquid and air velocity regions are in good agreement with transition criteria developed by Hibiki and Mishima (2001) even though their model was developed for upward flow. However, it was found that new criterion should be developed for flow pattern transition in low velocities of liquid and air.

INTRODUCTION

Many studies have been carried out on two-phase flow in vertical tubes and channels in last 50 years. Most of these studies were concerned with upward flow in vertical channel of medium size circular tube. Although there are great differences between upward and downward flow, studies on vertical upward flow are much more active than those on vertical downward flow in a channel. In addition, due to the increase of surface forces and friction pressure drop, the pattern of gas-liquid two-phase flow inside the rectangular channel is different from that in a circular tube. The downward flow in a rectangular channel is universally applicable to cool the plate type nuclear fuel in research reactors. The sub-channel of the plate type nuclear fuel is designed with a few millimeters of gap width. In this study, the flow regime for downward two-phase flow in narrow rectangular channels is proposed.

Wilmarth and Ishii [1][2] developed a flow regime for upward two-phase flow in rectangular channel with the gap width of 1 and 2 mm. They did comparative analysis of their data with flow regime transition criteria suggested by Mishima and Ishii [3], and added a new distribution parameter needed for the boundary of bubbly to slug flow transition. Xu [4] performed an experimental study on adiabatic upward air-water two-phase flow in rectangular channel with the gap widths of 0.3 mm, 0.6 mm and 1.0 mm. The flow regimes in those channels were similar to those found in the previous studies except the channel with the gap widths of 0.3 mm. In case of the gap widths of 0.3 mm, several new regions in flow regime are observed that are different from the previous studies. Hibiki and Mishima [5] measured flow regime, void fraction, velocity of slug bubble and pressure drop in rectangular channels with the gap widths of 1.0 mm, 2.4 mm and 5.0 mm. They developed the new flow regime transition criteria and compared it with the previous data for two-phase flow in narrow rectangular channels with the gap widths of from 0.3 mm to 17 mm. A new theory needs to be developed for narrow rectangular channels with the gaps under 0.3 mm. Experimental result of two-phase flow in rod bundles by Paranjape et al. [6], or annulus by Mishima and Ishii [3], Sun et al. [7], Julia et al. [8] is shown the cap-bubbly flow motions were found to be relatively steady in narrow gap region.

Oshinowo and Charles [9] investigated two-phase downward flow in a vertical annular channel and categorized flow patterns into six regions and developed a model with various fluid properties. Both Martin [10] and Kulov et al. [11] performed experimental research on the transition of bubbly to slug flow and slug to annular flow. The flow regime maps for downward two-phase flow covering a wide range are proposed by Usui and Sato [12], Spedding and Nguyen [13], Barnea et al. [14] and Kendoush and Al-Khatab [15]. Moreover, Barnea et al. [14], Usui [16] and Goda et al. [17] developed transition criteria models for the downward two-phase flow regimes. Julia et al. [18] and Swanand and Afshin [19] experimentally observed differences in the appearance of the upward and downward two-phase flow regime. And they concluded that it was the result of the interaction of the liquid inertia and the buoyancy force.

Most of these studies have researched the upward two-phase flow in the circular tube. Meanwhile, it was observed that there is scarcity of study on the investigation of the downward two-phase flow in the narrow gap rectangular channels in open literature, although the upward and downward two-phase flows

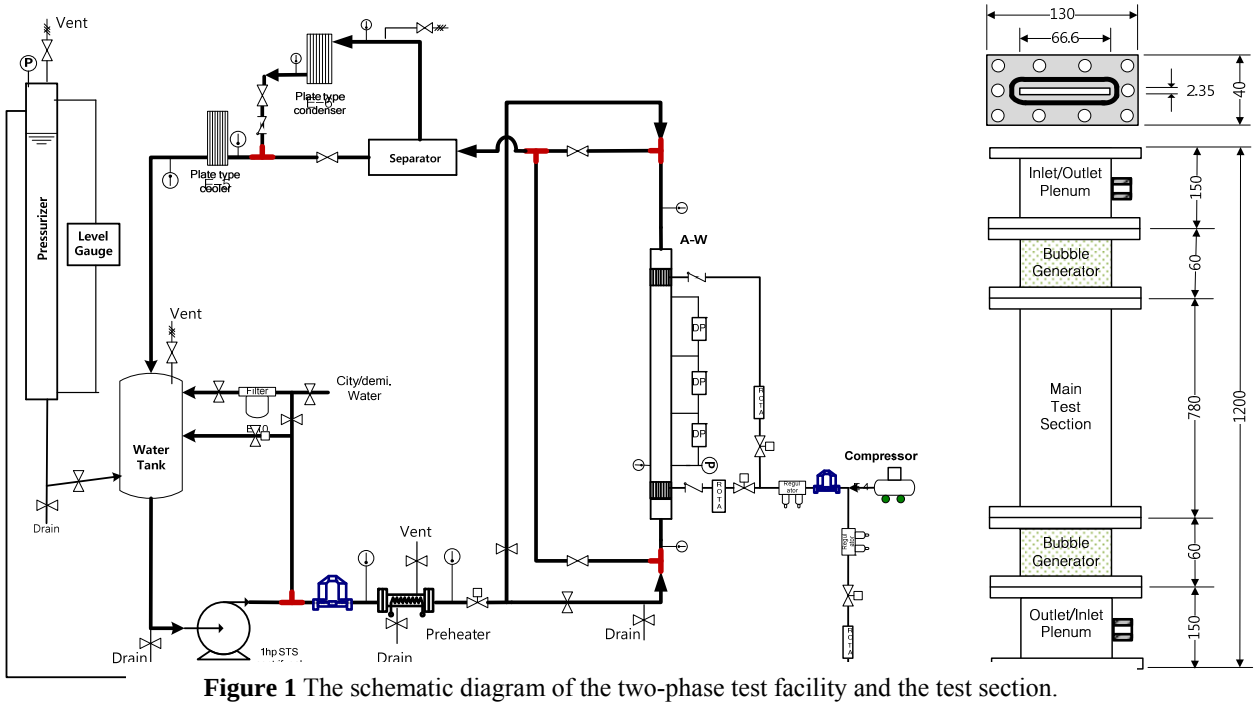

Figure 1 The schematic diagram of the two-phase test facility and the test section.

were observed to be different in terms of interaction of the buoyancy, gravity and liquid inertia forces. Therefore, this study suggests a new flow regime map for downward two-phase flow in vertical rectangular channels with the gap width of 2.35 mm. Measurements were taken using the high speed camera and these measurements were analyzed with image processing toolbox of Matlab. This study analyzes several regions such as bubbly, cap-bubbly, slug, churn-turbulent, annular and large bubble flow. Flow regime map suggested in this study has been compared with the upward two-phase flow regime criteria proposed by Hibiki and Mishima [5].

EXPERIMENTAL APPARATUS AND METHODS

Experimental Apparatus

The observation of air water two-phase flow pattern was performed in the closed loop apparatus. Figure 1 shows the schematic of the closed two-phase flow test apparatus and the test section. There is a vertical rectangular main test section, a pump, a pre-heater, a condenser, a cooler, a degassing system, measurement devices, and a control and data acquisition system in the test apparatus. The main test section consists of two bubble generators in up and down plenums and two transparent acrylic windows whose vertical lengths are 780 mm with the gap widths of 2.35 mm between them. Air is supplied by a compressor to the test section through bubble generators that involves a porous media with the pore size of 1 μm. In air-water two-phase flow experiments, ideally the bubble distribution is required to be uniform. Cross-sectional area of channel should be maintained during bubble movement. In contrast to upward flow, bubbles are moved to downward which affect buoyancy forces in channel area. Figure 2 shows the schematic of the bubble generators. The air is mixed in the water at the bubble generators and the air-water mixture moves downward into the test section. After running through the test section, the air is separated out at a separator into the atmosphere, and the water is continuously kept in circulation by the centrifugal pump. One coriolis flowmeter and a thermal mass flowmeter is used to measure the flow rate of the air. Also, a coriolis flowmeter is used to measure the flow rate of the water. The apparatus is able to control the vertical flow direction by the two ball valves located after passing the pre-heater. The flow rates at the test section are regulated by the valve installed between the pre-heater and the ball valves. The temperatures in the experimental apparatus and the inlet/outlet pressures of test section are measured using T-type thermocouples and pressure transmitters, respectively. The errors in the measurement of flow rates, temperature, and pressure are 0.1% of reading, 0.3 ℃, and 0.05% of span (3.0 kPa), respectively.

Visualization and Image Analysis

The images in the test section were recorded using a high speed digital video camera with a double laser source. Figure 3 represent schematic of flow pattern visualization system. The shadow image technique is applied for obtaining both the shape and the location of individual bubbles. In the test section, a high speed camera is utilized for performing the measurement of both phases. The trigger timings of the laser and a high speed camera are synchronized using a pulse generator supported by laser generation system. The recording frequency and resolution of the camera were set to 5,000 frames per second and 1024 × 512 pixels.

The high speed cameras capture RGB images with noise. But the extraction of bubble parameters requires binary images,

so it's necessary to transform the initial RGB images to binary. In this process, many kinds of digital image processing methods were used, such as type conversion of image, noise filtering, painting algorithms and edge detection. Images are stored as a matrix in which every element is the pixel value. Grayscale images only have the strength information in the images and binary images only have black and white which are referred using 0 and 1 respectively. In order to automate the image acquisition and data processing procedure, an in-house routine was developed using Matlab image processing toolbox, with which a large number of images were processed and bubble behavior estimated.

Image processing procedure involved following steps:

A. First step of image processing is to remove noise such as smudge marks in the backgrounds. In general, noise is removed to use filter such as linear filtering, median filter. As common kinds of linear filter, mean filter applies to filtering the grain noise in images. Median filter operates easily and can protect the boundary in images, especially it is effective for filtering the salt and pepper noise, but sometimes, thin lines and small target regions might be lost.

B. Afterwards grayscale images are converted into binary images. In the image processing, the key point is to find a threshold that can differentiate the two phases. In this paper, the difference between the target and the background of the bubble images is obvious, so the images could be binarized using the two-dimensional Otsu adaptive threshold algorithm. Hole in the bubbles might be generating due to refraction index difference between the phases while collection of images. Even after image filtering and binarization, these holes are still present. So the holes must be filled with image corrosion and dilation such that the edge detection could proceed effectively.

C. At Last, image processing is to fine the edge. In image, the edge refers to the end of a feature area and the beginning of another feature area. Edge detection actually is to detect the position where the images features have changed. The edge detection can be achieved based on grayscale images using the operator. The common operators for edge detection include differentiating operator, sobel operator, Laplacian of Gaussian operator and Canny operator. This study uses sobel operator to detect the bubble edge based on grayscale image.

EXPERIMENTAL RESULTS AND DISCUSSION

Flow Regime Classification

Also similar to the upward flow regimes, downward two-phase flow regimes are usually classified into four or five regions. But it is important whether downward two-phase flow regimes have considerable differences with upward flow regimes, with the cross-sectional shape change of the sub-channel. In this paper, two-phase flow regimes are classified into seven categories base on the average void fraction in downward rectangular channel.

Falling film flow and large bubble (LB) In low mass flow rates of gas and liquid, the falling film flow that the liquid phase streamed is observed at down near the wall. The flow pattern turns to be the annular flow with increasing the gas flow rates. When the liquid velocity increases, the bubbles gather together and flow pattern turns into the slug flow. On the contrary to this, the flow pattern becomes the bubbly flow when the liquid flow rates increases. When the superficial liquid velocity is less than 0.8 m/s and the superficial gas velocity is below 0.2 m/s in the bubbly flow development process, the bubble diameter for large bubble is close to the width of the channel. The bubbles sometimes coalesce into the large bubbles at a center of the channel. The large bubbles tend to stay at the center of the channel when the drag force and the inertia force working on the bubble are equilibrium. Figure 2(a) shows the image of large bubbles and (b) shows the averaged void fraction line of downward flow in rectangular channel.

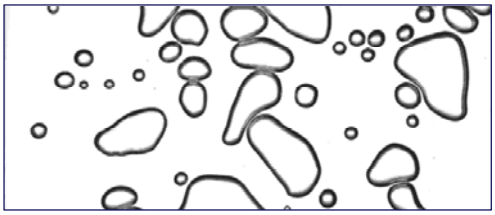

(a) Bubble shape

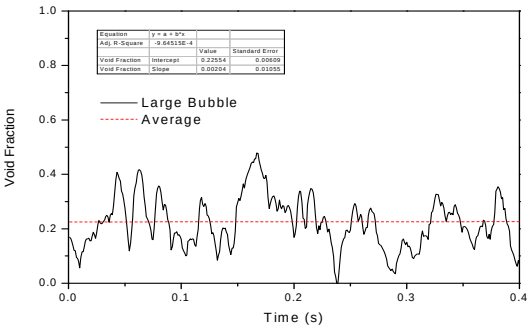

(b) Averaged void fraction

Figure 2 Bubble shape and void fraction of large bubbly flow

Bubbly flow (B) Due to the superficial liquid velocity increase, the large bubbles are dispersed into small bubbles. The bubbly flow is similar to that of the upward flow in circular tube. It is the significant difference observed in the bubbles in downward flow that the size is smaller than the gap of rectangular channels, and average void fraction is less than 0.25 Figure 3(a) and (b) show the image of bubbly flow and the line averaged void fraction of downward flow in rectangular channel, respectively.

Cap-bubbly flow (CB) Due to the a little gas flow rates increase, a number of bubbles caused a number of coalescence and the growing bubbles to be flattened and distorted to appear

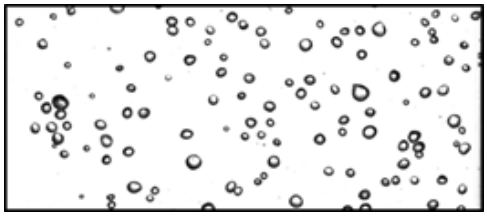

(a) Bubble shape

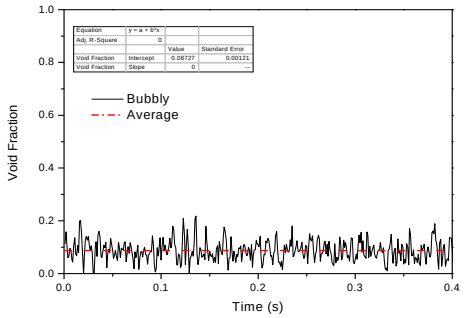

(b) Averaged void fraction

Figure 3 Bubble shape and void fraction of bubbly

as small overturned caps. The cap bubbles in downward flow are formed in low gas fraction condition by comparison with the upward flow case. In vertical downward flow, the buoyancy force is produced in opposition to the direction of gravity in the mean flow. While the low gas and liquid flow rates, the small slug bubbles shows similar shape of overturned caps. The transition from cap-bubbly to slug flow occurs at the void fraction of approximately 0.7. Figure 4(a) and (b) show the image of cap-bubbly flow and the line averaged void fraction in downward rectangular channel, respectively.

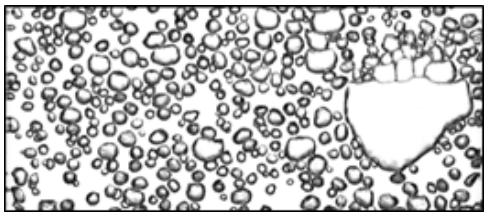

(a) Bubble shape

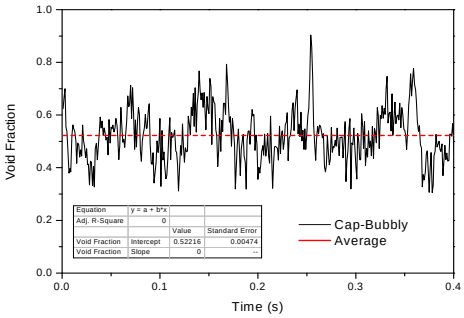

(b) Averaged void fraction

Figure 4 Bubble shape and void fraction of cap-bubble flow

Slug flow (S) The bubbly to slug flow transition criteria is generally used in a circular tube occurs at the void fraction of approximately 0.3 [1][10][14][17]. The slug flow observed in this study is far different from that observed in the upward flow at the narrow rectangular channel. Due to the small depth and relatively wide width of channel, the cap-bubble to slug transition occurs at the line averaged void fraction of approximately 0.7. The line averaged void fraction of slug flow was fluctuated by liquid slugs that bridge the test section. Figure 5(a) and (b) show the shape of slug flow and the line averaged void fraction in downward rectangular channels.

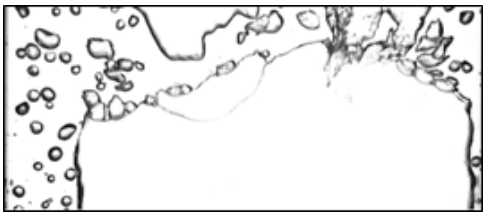

(a) Bubble shape

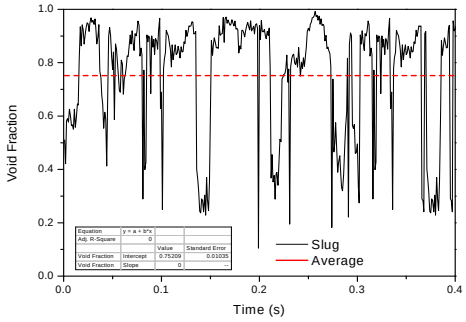

(b) Averaged void fraction

Figure 5 Bubble shape and void fraction of slug flow

Churn-turbulent flow (CT) When the gas flow rates increases, a breakdown in the slug flow makes the flow regime unstable. The combined liquid band is often broken up. This destroyed liquid lumps is accumulated, builds a bridge and is lifted by the gas again. Churn-turbulent flow usually shows this quicksilver liquid. The line averaged void fraction of churn-turbulent flow is close to slug flow .However churn-turbulent flow is lots more irregular, frothy and disordered than that of slug flow. Figure 6(a) and (b) show the image of churn-turbulent flow and the line averaged void fraction in downward rectangular channel.

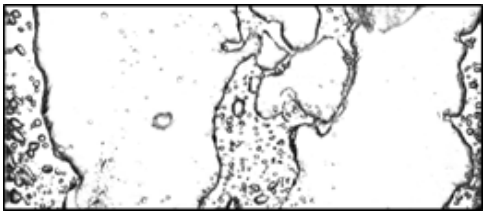

(a) Bubble shape

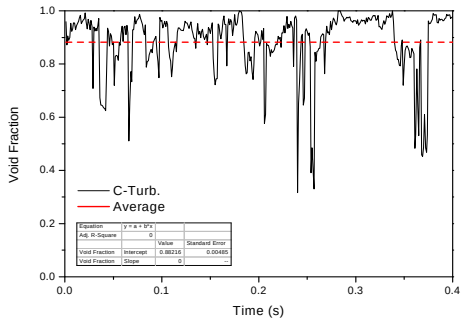

(b) Averaged void fraction

Figure 6 Bubble shape and void fraction of churn-turbulent flow

Annular flow (A) The gas phase flow is located in the center of the channel in an unbroken line and the liquid phase flow near the widely side wall of the channel makes film. The gas flow entrains the liquid phase as small droplets, but it is quite uncommon for bubbles to be entrained in the liquid side. Figure 7(a) and (b) show the image of annular flow and the line averaged void fraction in downward rectangular channel.

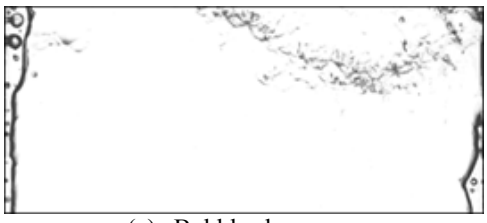

(a) Bubble shape

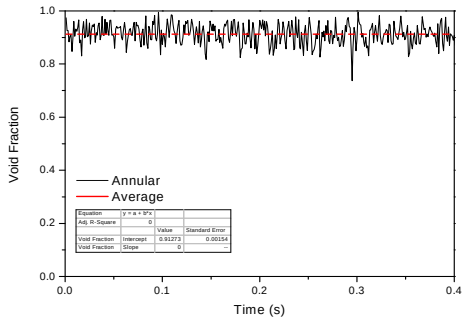

(b) Averaged void fraction

Figure 7 Bubble shape and void fraction of annular flow

Flow Regime Map

Flow regime map in the rectangular channel with the depth of 2.35 mm is separated into six regions using void fraction as shown above. In the flow regime map, the 60 cases of downward flow conditions with superficial gas velocity ranging from 0.02 to 8 m/s and superficial liquid velocity ranging from 0.5 to 2.5 m/s were analyzed. Figure 8 shows the flow regime map. Dot lines on the flow regime map are transition criteria of the vertical upward flow in the narrow rectangular channel suggested by Hibiki and Mishima [5]. The general transition criteria aspect of the experimental results is similar to that of Hibiki and Mishima [5].

Figure 8 shows the experimental data of the transition criteria by Hibiki and Mishima [5]. The experimental result of the downward flow regime in rectangular channel in this study is similar to transition criteria suggested by Hibiki and Mishima [5] investigated in vertical upward flow though they are in opposing directions. The flow regime studied in recent years showed that the transition criteria in the upward flow could be substitutable for that in the downward flow in relatively high superficial liquid velocities over 1 m/s.

However, at superficial liquid velocity below 0.8 m/s, a new model is needed for the criteria in the flow regime for the downward flow in narrow rectangular channel. Furthermore, the results in this experimental study showed that the cap-bubbly flow region appears in the region that is classified into slug flow region by Hibiki and Mishima [5]. Moreover, the cap bubbles in downward flow are formed in lower gas fraction than in the upward flow. This phenomenon is occurred because the opposite direction between inertial and buoyancy force that increases the bubble coalescence in downward flow. Barnea [18] researched modified model for the transition affected by inclination angle. According to his study, at superficial liquid velocity below 1 m/s, the two-phase flow is affected by the buoyancy force. In recent study said that at superficial liquid velocity approximately 0.3 m/s, the gas phase flow is continuous at center of the channel. And the liquid phase flows following both sides of the wall of channel. When the superficial liquid velocity is from 0.5 to 0.8 m/s, the bigger bubble size and the lower bubble velocity are observed while the superficial liquid velocity is over 1.0 m/s on the wall.

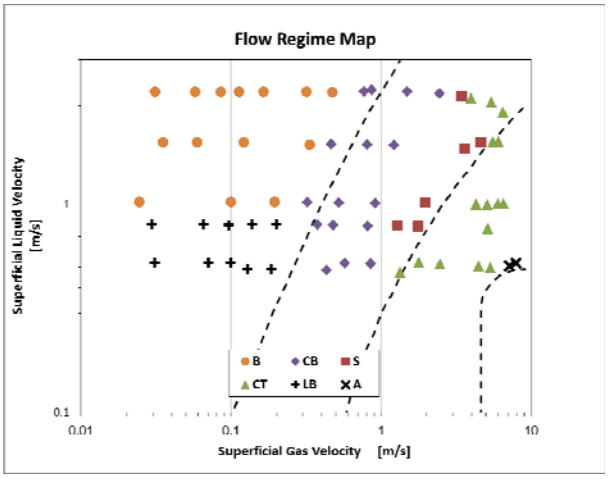

Figure 8 Two-phase flow regime map for downward flow in rectangular channel

CONCLUSION

In this study, the vertical downward two-phase flow is investigated in a narrow rectangular channel with gap width of 2.35 mm and compared to previous flow regime map. The basic

concept of the flow regime is in such a way that of Wilmarth and Ishii [1] suggested for the upward flow in rectangular channel. The flow regime was classified into seven patterns by the line averaged void fraction such as falling film, large bubbly, bubbly, cap-bubbly, slug, churn-turbulent and annular flows using the high speed camera image.

The experimental data have been compared and analyzed with the results of Hibiki and Mishima [5]. The downward flow regime has shown similar aspect to transition criteria developed by Hibiki and Mishima [5] in upward two-phase flow. When the liquid velocity is relatively high, over 1 m/s, the transition criteria for the upward flow can be substituted for the downward flow. In the experimental data, two major differences are observed between the downward and the upward flow in the rectangular channel. Firstly, the cap-bubbly flow appears at the region that Hibiki and Mishima [5] classified into slug flow in the flow regime map. Secondly, in the superficial liquid velocity from 0.5 to 0.8 m/s, the bigger bubble size and the lower bubble velocity are observed while the superficial liquid velocity is over 1.0 m/s on the wall. In superficial liquid velocity below 1 m/s, a new model is needed for the transition criteria for the cap-bubbly flow regime in the downward flow.

REFERENCES

[1] Wilmarth T., and Ishii M., Two-phase flow regimes in narrow rectangular vertical and horizontal channels, *International Journal of Heat and Mass Transfer*, Vol. 37, 1994, pp. 1749-1758

[2] Wilmarth T., and Ishii M., Interfacial area concentration and void fraction of two-phase flow in narrow rectangular vertical channels, *Journal of Fluids Engineering*., Vol. 19,1997, pp. 916-922

[3] Mishima K., and Ishii M., Flow regime transition criteria for upward two-phase flow in vertical tubes, *International Journal of Heat and Mass Transfer,* Vol. 27, 1984, pp. 723-737

[4] XU J., Experimental study on gas–liquid two-phase flow regimes in rectangular channels with mini gaps, *International Journal of Heat and Fluid Flow*, Vol. 20, 1999, pp. 422-428

[5] Hibiki T., and Mishima K., Flow regime transition criteria for upward two-phase flow in vertical narrow rectangular channels, *Nuclear Engineering and Design*, Vol. 203, 2001, pp. 117-131

[6] Oshinowo T., and Charles M.E., Vertical two-phase flow. Part I. Flow pattern correlations, *The Canadian Journal of Chemical Engineering*, Vol. 52, 1974, pp. 25-34

[7] Martin C.S., Vertically downward two-phase slug flow, *Journal of Fluids Engineering-Transaction of the ASME*, Vol. 98, 1976, pp. 715-722

[8] Kulov N.N., et al., Pressure-drop, mean film thickness and entrainment in downward two-phase flow, *Chemical Engineering Journal*, Vol. 18, 1979, pp. 183-188

[9] Usui K., and Sato K., Vertically downward two-phase flow, (I). Void distribution and average void fraction, *Journal of Nuclear Science and Technology*, Vol. 26, 1989, pp. 670-680

[10] Spedding P.L., and Nguyen V.T., Regime maps for air water two-phase flow, *Chemical Engineering Science,* Vol. 35, 1980, pp. 779-793

[11] Barnea D., et al., Flow pattern transition for vertical downward two-phase flow, *Chemical Engineering Science,* Vol. 37, 1982, pp. 741-744

[12] Dendoush A.A., and Al-Khatab A.W., Experiments on flow characterization in vertical downward two-phase flow, *Experimental Thermal and Fluid Science*, Vol. 9, 1994, pp. 34-38

[13] Usui K., Vertically downward two-phase flow, (II). Flow regime transition criteria, *Journal of Nuclear Science and Technology*, Vol. 26, 1989, pp. 1013-1022

[14] Goda H., et al., Drift-flux model for downward two-phase flow, *International Journal of Heat and Mass Transfer*, Vol. 46, 2003, pp. 4835-4844

[15] Julia J.E., et al., Local flow regime analysis in vertical co-current downward two-phase flow, *Experimental Thermal and Fluid Science*, Vol. 44, 2013, pp. 345-355

[16] Swanand M.B., and Afshin J.G., Similarities and differences in the flow patterns and void fraction in vertical upward and downward two-phase flow, *Experimental Thermal and Fluid Science,* Vol. 39, 2012, pp. 213-227

[17] Taitel Y., et al., Modelling flow pattern transitions for steady upward gas–liquid flow in vertical tubes, *AIChE Journal,* Vol. 26, 1980, pp. 345-354

[18] Barnea D., A unified model for prediction flow pattern transitions in the whole range of pipe inclination, *International Journal of Multiphase Flow,* Vol. 13, 1978, pp. 1-12

EXPERIMENTAL STUDIES OF HEAT TRANSFER COEFFICIENT AND PRESSURE DROP IN INCLINED CONDENSING UNITS

Adelaja A.O.*, Dirker J.** and Meyer J.P. ***
*Author for correspondence
Department of Mechanical and Aeronautical Engineering,
University of Pretoria,
Pretoria, 0002,
South Africa,
E-mail: *adekunle.adelaja@up.ac.za **jaco.dirker@up.ac.za ***josua.meyer@up.ac.za

ABSTRACT

This paper presents the experimental heat transfer coefficient and frictional pressure drop values during the condensation of R134a inside a smooth copper tube for vapour qualities of 0.25, 0.5 and 0.75, mass fluxes of 200 kg/m^{2}s to 300 kg/m^{2}s, saturation temperatures of 30°C and 40°C and tube inclination angles ranging between -90° (vertical downward) and +90° (vertical upward). The effects of the inclination angle coupled with mean vapour quality, mass flux and saturation temperature were investigated on the heat transfer coefficient and pressure drop. An entropy generation analysis was conducted to determine at which inclination angle entropy generation is minimised. It appears as if entropy generation was at its lowest for vertical upward flow, but that for some cases this was also achieved for slightly downward flow.

INTRODUCTION

Condensation heat transfer and pressure drops are very important parameters for consideration in the effective and efficient design of condensing heat exchangers. For heat exchanger design and process engineers the interest is focussed on enhanced heat transfer coefficient and reduced pressure drop in the equipment, be it either the condenser or the evaporator. Enhanced heat transfer improves the thermal performance of the heat exchanger. Reducing the pressure drop, however, causes a reduction in the pumping power requirement of the cycle resulting in reduction in the compressor or pump design size which corresponds to lower cost.

Most techniques proposed to enhance the heat transfer coefficient are unfortunately accompanied by increased local pressure penalty factors. This is apart from the increased cost of production of the enhanced tubes in case of passive methods, or the additional external power which had to be applied in active heat enhancement techniques [1]. For instance, for spiral microfins, the heat transfer enhancement is between 80% and 180%, the pressure penalty factor is between 20% and 80% while for cross groove tubes the heat enhancement is between 25% and 30% while the pressure penalty factor is between 6% and 10 % [2]. Thus, the aims of new convection heat transfer methods are the reduction of pressure drop, increase of the overall thermal efficiency, and reduction of the capital cost of such systems. It is known that the inclination angle of the condenser tubes in condensation devices have an impact on the two-phase flow pattern distribution which influences the heat transfer coefficient and the effective pressure drop. Inclined tubes are especially of interest in the A- and V-frame condensers. Several studies [3-8] have been conducted on the heat transfer coefficient of in-tube condensation of R134a at different inclination angles, but few have been conducted dedicated to pressure drop [9-10]. To the best of the authors' knowledge the application of these design parameters in term of the influenced of the inclination angle to aid process and heat exchanger design engineers and researchers in their activities is scarce in open literature. Akhavan-Behabadi *et al.* [11] considered in their study condensation heat transfer coefficients of R134a in microfin tubes of an inner diameter of 8.92 mm at

NOMENCLATURE

A	[m^2]	Area
d	[m]	Diameter
ΔP	[kPa]	Differential pressure
g	[ms^{-2}]	Gravitational acceleration
G	[kgm^{-2}s]	Mass flux
k	[Wm^{-1}K^{-1}]	Thermal conductivity
L	[m]	Length
ΔP_{fric}	[Pa]	Frictional pressure drop
Q	[W]	Heat transfer rate
R	[KW^{-1}]	Thermal resistance
$s_{gen,\Delta P}$	[J/kgK]	Specific entropy generation due to pressure drop
$s_{gen,Q}$	[J/kgK]	Specific entropy generation due to heat transfer
T	[K]	Temperature
$\bar{T}$	[K]	Mean temperature
x	[-]	Vapour quality
z	[-]	Axial direction

Special characters

α	[Wm^{-2}K^{-1}]	Heat transfer coefficient
β	[°]	Inclination angle
ε	[-]	Void fraction
ρ_{TP}	[kgm^{-3}]	Density

Subscripts

Cu	Copper
i	Inner
j	Measurement location
local	Specific position
m	Mean
o	Outer
out	Outlet
sat	Saturation
test	Test
w	Wall

mass fluxes (G) between 59 kg/m^{2}s and 107 kg/m^{2}s, saturation temperatures (T_{sat}) between 26°C and 32°C, mean vapour qualities between 0.2 and 0.8 and inclination angles (β) ranging between -90° and +90°. They reported enhanced heat transfer which was optimised at an upward inclination of 30°. Sapali and Patil [12] conducted an experimental investigation of heat transfer coefficient of R134a and R404a inside a horizontal smooth tube with an inner diameter of 8.56 mm and a microfin tube with an inner diameter of 8.96 mm for mass fluxes between 90 kg/m^{2}s and 800 kg/m^{2}s and saturation temperature between 35° and 60°. The heat transfer enhancements obtained in the microfin tube were between 50% and 150% for R134a and between 30% and 100% for R404a. In most of the works on microfin tubes the area ratio (AR) is greater than unity.

Lyulin *et al.* [13] experimentally investigated the condensation heat transfer coefficient of pure ethanol in a smooth tube at a saturation temperature of 58°C. They stated that the heat transfer coefficient reduces with increased temperature difference between the saturation and wall temperatures. They formally reported optimised inclination effect on heat transfer coefficient at between -15° and -35°. Lips and Meyer [3, 4 and 9] in their experiments on condensation heat transfer coefficient and pressure drop of R134a in a smooth copper tube with an inner diameter of 8.38 mm operated at mass fluxes between 200 kg/m^{2}s and 600 kg/m^{2}s, mean vapour qualities between 0.1 and 0.9, and inclination angles between -90° and +90° for T_{sat} = 40°C obtained optimised inclination angles between -15° and -30°. The heat transfer changed by up to 43% in terms of inclination with respect to the horizontal tube inclination heat transfer coefficient. They also observed that the pressure drop increased with mass flux and vapour quality for $-90° \leq \beta < +30°$ but decreased with mean vapour quality for $+30° \leq \beta \leq +90°$. Meyer *et al.* [5] and Adelaja *et al.* [6-8] extended the work of Lips and Meyer in various experimental results at different saturation temperatures. In addition to the conclusions of Lips and Meyer, they stated that both heat transfer coefficient and pressure drop decreased with saturation temperature. It is, however, interesting to have a holistic view of the heat transfer and pressure drop in an inclined smooth tube to serve as a guide for heat exchanger design, process engineers and researchers who are not only interested in heat transfer enhancement, but also in the reduction in pressure drop.

In this study, it is shown that in the gravity dominated flow regime, there could be heat enhancement accompanied by reduced penalty factor without an increase in heat transfer surface area. This could be achieved by inclining the equipment relative to the horizontal causing the two-phase flow refrigerant subject to the influence of gravity.

EXPERIMENTAL SET-UP

The present study was conducted at the test facility in the laboratories of the Department of Mechanical and Aeronautical Engineering, University of Pretoria, South Africa (Figure 1). The test set-up allowed for double tube condensation heat transfer and pressure drop data to be collected over a wide range of operating conditions. The setup comprised of three flow loops: the refrigerant, the cooling water and the hot water

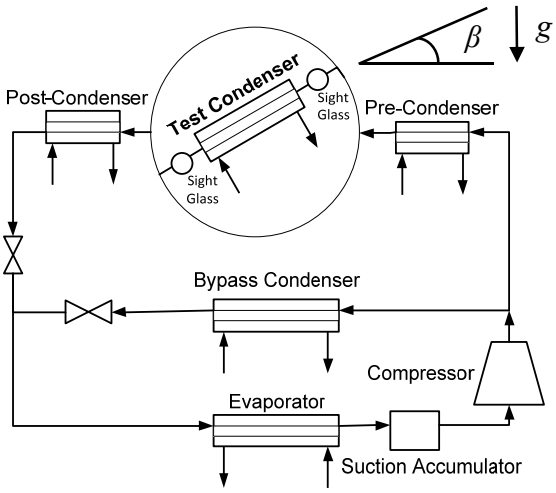

Figure 1 Schematic diagram of the test rig.

loops. In the refrigerant loop, there were two high-pressure lines. The first line contained the pre, test and post condensers, while the second line contained the bypass condenser which was employed to assist in regulating the amount of refrigerant trough the test condenser.

In the high pressure test line, superheated vapour from the 10 kW hermetically sealed scroll compressor entered into the pre-condenser and was partially condensed. The vapour quality achieved at the outlet of the pre-condenser was equal to the inlet vapour quality to the test condenser because the connection interface between the two condensers was adiabatic. The refrigerant entered the test condenser, which carried the refrigerant in an inner tube and water in annulus in a counter flow arrangement, at a prescribed mass and inlet vapour quality. Here, the refrigerant vapour condensed further in the test tube at a prescribed heat flux as controlled via the local cold water flow rate. In this study this heat flux was maintained between 230 W and 270 W. More information on the test condenser is supplied in the next section. The partially condensed liquid-vapour mixture left the test condenser and was fully condensed in the post-condenser. The post condenser ensured that the two-phase mixture became fully liquid before reaching the electronic expansion valve (EEV). Liquid refrigerant from the two high-pressure lines were combined and flowed to the evaporator where warm water from the hot water flow loop was used to evaporate the liquid refrigerant before the vapour passed to the compressor via the accumulator. All heat exchangers (including all condensers and the evaporator) where of the double pipe kind and were operated in counter flow arrangements with the refrigerant flowing in the inner tube and water flowing in the outer annular space. All water and refrigerant flow rates were measured by Coriolis flow meters.

For the water loops, a 50 kW cooling and 70 kW heating dual function heat pump supplied cold and hot water via a distribution system. The cold and hot water temperatures were thermostatically controlled to be between15^{o}C and 25°C, and 40^{o}C respectively deepening on the test conditions. Thermal buffering was obtained by using two 5000 litre insulated water reservoirs to store the hot and cold water.

TEST SECTION

The test section had a heat transfer length of L = 1.488 m. It was a double pipe counter flow condenser constructed from hard drawn copper with water as a coolant in the annulus. The refrigerant vapour condensed inside the inner tube. The inner tube had an inner diameter of d_i = 8.38 mm and an outer diameter of d_o = 9.55 mm while the annulus had an outer diameter of 15.9 mm. The connections to the test condenser were made of flexible pressure hoses. These enabled the test section to rotate about two fixed hinges. To ensure that the flow through the test section was fully developed, a straight calming section, 50 diameters long was situated at the entrance.

All temperature measurements were done with T-type thermocouples calibrated against a high precision Pt-100 resistant temperature detector to an accuracy of 0.1°C. On the test condenser, thermocouples were arranged such that the tube wall temperature ($T_{w,o}$) could be measured. At each location four thermocouples were installed and spaced 90° to each other around the tube (i.e. top, bottom and two sides). Twenty-eight such thermocouples were installed in small pot holes drilled at seven equal-distant positions on the inner tube. Two absolute pressure transducers were connected between the inlet and outlet of the test section so that the absolute pressure recording used was the average of the two pressure readings. The pressure was used as the saturation pressure (accurate to ±0.25% of the full scale). The measured value when used with the condensation curve provided by REFPROP [14] gave the saturation temperature which was verified by direct measurement. The difference in the two values was found to be around 0.1°C. The pressure drop across the test section was measured by a differential pressure transducer (FP 2000 Sensotec) which was calibrated to an accuracy of ±0.05 kPa.

At the inlet and outlet of the test section were two sight glasses which enabled flow visualization and also served as insulators against axial heat conduction. A high speed camera was installed at the outlet sight glass and was used to record and document the flow patterns.

EXPERIMENTAL PROCEDURE AND DATA REDUCTION

The test conditions described in Table 1 give the range of experimental variables used in this study and their control fluctuations. The mean vapour quality, x_m, is based on the arithmetic average between the entrance and exit qualities, x_{in} and x_{out} respectively of the R134a as obtained by using the energy balance principle for the pre-condenser and test-condenser. After steady state conditions were reached, the different sensor signals were recorded continuously through the Labview and National Instrument data acquisition system for about a period of 10 minutes. In order to avoid noise measurement, the average of the points was used for the calculations of the fluid properties, heat transfer coefficients, and other parameters of interest.

The convective heat transfer coefficient in the test condenser was calculated from Newton's law of cooling:

Table 1 Experimental variables and fluctuations.

Parameter	Range	Fluctuations
T_{sat}	30°C and 40°C	± 0.6°C
G	200 and 300 kg/m^{2}s	± 5 kg/m^{2}s
x_m	0.25, 0.5, 0.75	± 0.01
β	-90° to +90°	± 0.1°

$$\alpha = \left| \frac{Q_{test}}{A(\overline{T}_{w,i} - T_{sat})} \right| \quad (1)$$

Here Q_{test} is the heat transfer rate in the test condenser as obtained via the energy equation on the water side based on the measured inlet and outlet water temperatures and the water mass flow rate. A is the inner surface area of the inner tube of the test condenser. T_{sat} is the mean of the saturation temperature between the inlet and outlet of the section. $\overline{T}_{w,i}$ is the calculated mean inner wall temperature based on the measured mean outer wall temperature of the tube $\overline{T}_{w,o}$ through the thermal resistance of the wall of the copper tube, R_w

$$\overline{T}_{w,i} = \overline{T}_{w,o} + \left| Q_{test} R_w \right| \quad (2)$$

Here $R_w = \ln(d_o/d_i)/2\pi k_{Cu} L$ with k_{Cu} referring to the thermal conductivity of the copper wall. $\overline{T}_{w,o}$ was calculated using the trapezoidal numerical integration:

$$\overline{T}_{w,o} = \frac{1}{L} \sum_{j=1}^{6} \left[\left(T_{w,o}^{j} + T_{w,o}^{j+1} \right) \left(z_{j+1} - z_j \right) \right] \quad (3)$$

where $T_{w,o}^{j}$ is the average temperature at the j^{th} location of the seven different stations and $z_{j+1} - z_j$ is the distance between the measurement locations.

RESULTS AND DISCUSSION

Heat Transfer Coefficient

In Figures 2 to 4 some heat transfer coefficient results are presented. Generally, it was found that the heat transfer coefficient increases with mass flux and mean vapour quality, but decreases with saturation temperature. It was further found that relative to the value at the horizontal inclination, there is enhancement in the heat transfer coefficient between the inclination angle of -15° and -30°. Figure 2 presents the result of experimental data for T_{sat} = 40°C for different G and x_m = 0.5. For G = 200 kg/m^{2}s, the flow pattern is within the gravity influenced regime (stratified-wavy) while for G = 300 kg/m^{2}s, the flow is annular-wavy.

On closer inspection it can be seen that the highest heat transfer coefficient occur between -15° and -30° during which there is a reduction in the liquid film thickness thus reduction in the thermal resistance of the film to heat transfer.

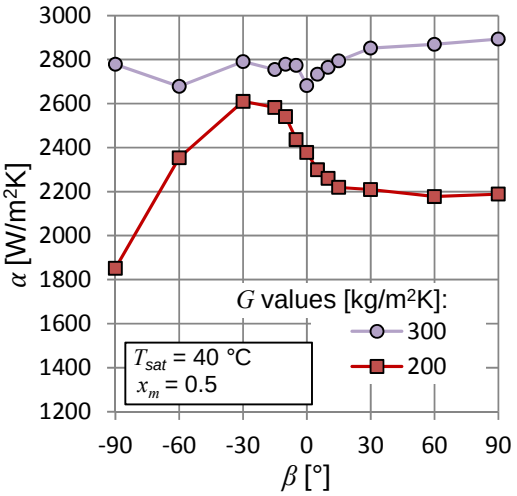

Figure 2 Inclination effect on heat transfer coefficient for different G for T_{sat} = 40°C, x_m = 0.5.

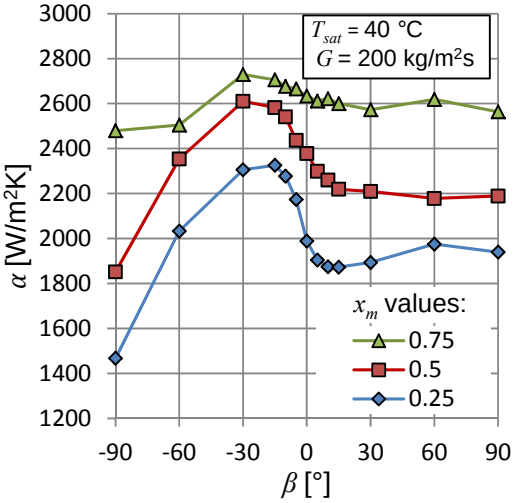

Figure 3 Inclination effect on heat transfer coefficient for different x_m for G = 200 kg/m^{2}s and T_{sat} = 40°C.

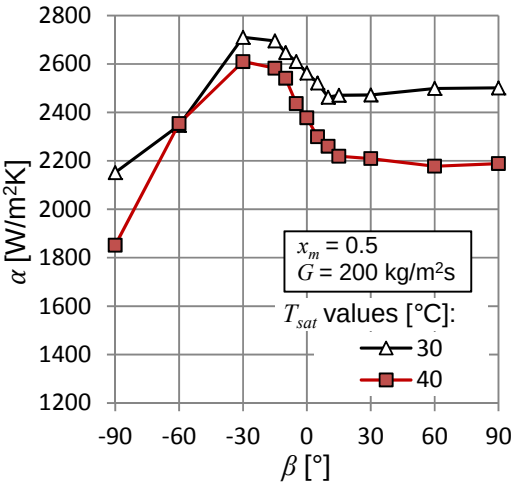

Figure 4 Inclination effect on heat transfer coefficient for different T_{sat} for G = 200 kg/m^{2}s and x_m = 0.5.

Figure 3 shows the influence of the vapour quality on the heat transfer coefficient at G = 200 kg/m^{2}s. Higher vapour qualities result in higher heat transfer coefficients. The figure also indicates that the highest heat transfer coefficients are present during slightly downward inclined tubes irrespective of the vapour quality, and that the lowest heat transfer coefficients were obtained for vertical downward flow (β = -90°). Figure 4 gives a comparison on the effect of the saturation temperature at G = 200 kg/m^{2}s and x_m = 0.5. It reveals that the optimal inclination angle occur during downward flow for β = -30° for T_{sat} = 30°C and for β = -15° for T_{sat} = 40°C. In general lowest heat transfer coefficients where achieved at vertical downward flow for both of these temperatures.

Frictional Pressure Drop

Figures 5 to 7 contain the frictional pressure drop, ΔP_{fric}, in the test section as obtained from experimental differential pressure measurement by using the void fraction model of Bhagwat and Ghajar [14]. The effects of the static pressure difference which changes according to the inclination angle are thus removed, along with the lesser effects of the momentum pressure differences. In Figure 5 it can be seen that both the mass flux and inclination angle affect the frictional pressure drop. For both mass flux cases there was a local minimum in the frictional pressure drop at an inclination angle of 0°. However, in general it appears as if the upwardly inclined tube cases had lower frictional pressure drops. These pressure drop variations can be linked to the flow pattern map, but is not discussed here due to space limitations.

In Figure 6 it can be seen that the vapour quality has a significant effect on the frictional pressure drop. Higher vapour qualities resulted in higher frictional pressure drops. In general, lower pressure drops were obtained for upwardly inclined flow. For vapour qualities of 0.5 and 0.75 the lowest frictional pressure drop was achieved during vertical upward flow, while for a vapour quality of 0.25 the frictional pressure drop appears to be present in horizontal tubes.

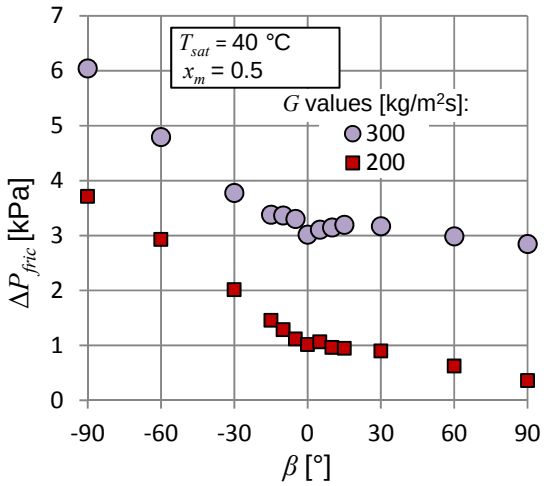

Figure 5 Inclination effect on pressure drop for different G for T_{sat} = 40°C and x_m = 0.5.

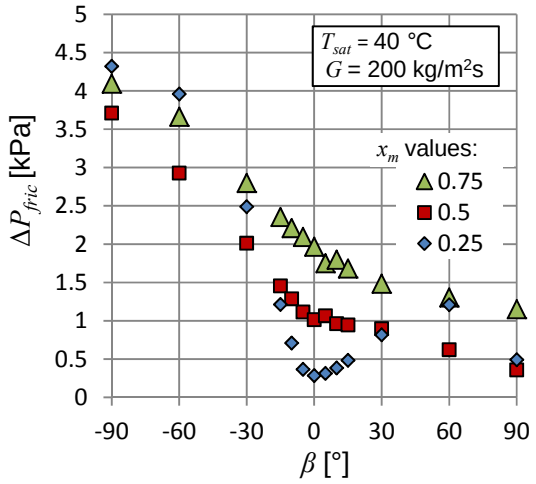

Figure 6 Inclination effect on pressure drop for different x_m for G = 200 kg/m^{2}s and T_{sat} = 40°C.

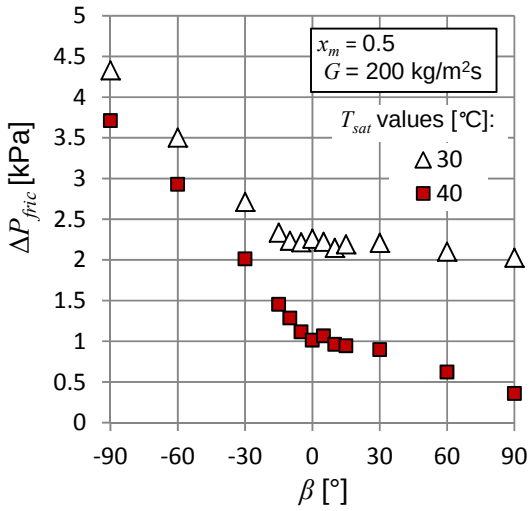

Figure 7 Inclination effect on pressure drop for different T_{sat} for G = 200 kg/m^{2}s and x_m = 0.5.

In Figure 7 it can be seen that higher frictional pressure drops were obtained for a saturation temperature of 30°C, as compared to a saturation temperature of 40°C. For both cases a slight local minimum in the frictional pressure drop was observed for horizontal tube orientations.

In all the cases considered here, vertical downward flow resulted in the highest frictional pressure drop. This was also the orientation that has the lowest heat transfer coefficient.

ENTROPY GENERATION ANALYSIS

The combined effect of inclination on the heat transfer coefficient and frictional pressure drop is presented in in this section. In order to make a comparison of the overall effects, entropy generation due to these two phenomena are considered for the two-phase flow passing through the test section. It must be noted that an entropy analysis done in isolation for a heat transfer tube, may not indicate the optimum system operating point, as this should be determined by considering the

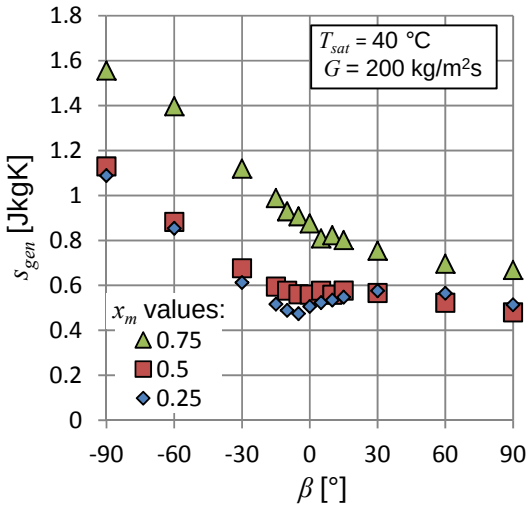

Figure 8 Inclination effect on total entropy generation for different x_m for G = 200 kg/m^{2}s and T_{sat} = 40°C.

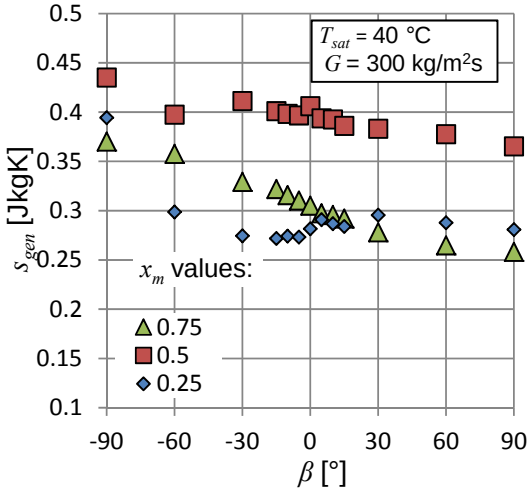

Figure 9 Inclination effect on total entropy generation for different x_m for G = 300 kg/m^{2}s and T_{sat} = 40°C.

entire system operation in which such a tube may be employed. It is done here only for discussion purposes.

The specific entropy generation associated with the frictional pressure drop, $s_{gen,\Delta P}$, can be expressed as follows:

$$s_{gen,\Delta P} = \frac{\Delta P}{\rho_{TP} T_{sat}} \tag{4}$$

Here the two-phase density, ρ_{TP}, of the mixture can be written as a function of the liquid and vapour phase densities, ρ_l and ρ_v, respectively and the void fraction, ε:

$$\rho_{tp} = \rho_l(1-\varepsilon) + \rho_v \varepsilon \tag{5}$$

The specific entropy generation associated with the heat transfer occurring at the tube wall over a temperature difference, $s_{gen,Q}$, can be expressed as follows:

$$s_{gen,Q} = h_{fg}\left(x_{in} - x_{out}\right)\left(\frac{1}{T_{w,i}} - \frac{1}{T_{sat}}\right) \quad (4)$$

Here, h_{fg} is the enthalpy of vaporisation and both temperatures are expressed in kelvin. The total entropy generation inside the test section, s_{gen}, is expressed by adding $s_{gen,\Delta P}$, and $s_{gen,Q}$.

Figures 8 and 9 show the influence of the inclination and vapour quality on the total entropy generation in the tube for mass fluxes of 200 kg/^{2}s and 300 kg/m^{2}s respectively for a saturation temperature of 40°C. It can be seen that for some of these test cases (x_m = 0.25 for both mass fluxes) there is an opportunity for entropy minimization at an inclinations angle of approximately -30° to -5°. However, in general terms, based on the data it appears as if entropy generation is at its lowest at vertical upward flow. For the 200 kg/^{2}s cases, higher vapour qualities resulted in higher entropy generation rates, while for the 300 kg/^{2}s cases, a clear dependence on the vapour quality could not be obtained. Similar type trends were observed at a saturation temperature of 30°C.

CONCLUSIONS

This study considered the heat transfer and frictional pressure drop in an inclined tube for condensation of R134a. These aspects are of particular importance to heat exchanger design engineers. It was found that slightly downward inclined tubes exhibited the highest heat transfer coefficient, while frictional pressure drops where generally lower for vertical upward flows. In certain cases a local minimum in the frictional pressure drop was obtained at horizontal tube orientations. An entropy generation analysis was conducted to determine the overall effect of the heat transfer enhancement and the pressure drop penalty on component level. It was found that entropy generation was minimised for some cases at slightly downward inclined flow, but for most cases the lowest entropy generation was obtained for vertical upward flow.

FURTHER NOTE

These results are based on the Bhagwat and Ghajar [14] void fraction correlation. Other void fractions correlations should also be considered.

ACKNOWLEDGMENTS

The funding obtained from the NRF, TESP, University of Stellenbosch/ University of Pretoria, SANERI/SANEDI, CSIR, EEDSM Hub and NAC is acknowledged and duly appreciated.

REFERENCES

[1] Siddique, M., Khaled, A-R.A., Abdulhafiz, N.I. and Boukhary, A.Y, Recent Advances in Heat Transfer Enhancements: A Review Report, *International Journal of Chemical Engineering,* Vol. 2010, 2010, Article ID 106461, pp. 1- 28.

[2] Cavallini, A., Del Col, D., Doretti, L., Longo, G.A., and Rossetto, L., Heat transfer and pressure drop during condensation of refrigerants inside horizontal enhanced tubes, *International Journal of Refrigeration,* Vol. 23, 2000, pp. 4-25.

[3] Lips, S., Meyer, P.J., Experimental study of convective condensation in an inclined smooth tube. Part 1: inclination effect on flow pattern and heat transfer coefficient, *International Journal of Heat and Mass Transfer,* Vol. 55, 2012a, pp. 395-404.

[4] Lips, S., Meyer, P.J., Stratified flow model for convective condensation in an inclined tube, *International Journal of Heat and Fluid Flow,* Vol. 36, 2012b, pp. 83-91.

[5] Meyer, J.P., Dirker, J., Adelaja, A.O., Condensation heat transfer in smooth inclined tubes for R134a at different saturation emperatures, *International Journal of Heat and Mass Transfer*, Vol. 70, 2014, pp. 515-525.

[6] Adelaja, A.O., Dirker, J., Meyer, J.P., Condensing heat transfer coefficients for R134a at different saturation temperatures in inclined tubes, *Proceedings of the ASME2013 Summer Heat Transfer Conference* (HT 2013 - 17375), Minneapolis, MN, 2013, pp. 1- 9.

[7] Adelaja, A.O., Dirker, J., Meyer, J.P., Convective condensation heat transfer of R134a in tubes at different inclination angles, *International Journal of Green Energy*, (In press).

[8] Adelaja, A.O., Dirker, J., Meyer, J.P., Experimental studies of condensation heat transfer in an inclined microfin tube, *Proceedings of the 15th International Heat Transfer Conference, IHTC-15,* Kyoto, Paper number 9361, 10 – 15 August, 2014.

[9] Lips, S., Meyer, P.J., Experimental study of convective condensation in an inclined smooth tube. Part II: inclination effect on pressure drops and void fractions, *International Journal Heat and Mass Transfer,* Vol. 55, 2012c, pp. 405-412.

[10] Adelaja, A.O., Dirker, J., Meyer, J.P., experimental investigation on pressure drop and friction factor in tubes at different inclination angles during the condensation of R134a, *Proceedings of the 15th International Heat Transfer Conference, IHTC-15,* Kyoto, Paper number 9363, 10 – 15 August, 2014.

[11] Akhavan-Behabadi, M.A., Kumar, R. and Mohseni, S.G., Condensation heat transfer of R 134a inside a microfin tube with different tube inclinations, *International Journal of Heat and Mass Transfer,* Vol. 50, 2007, pp. 4864 - 4871.

[12] Sapali, S.N., Patil, P. A., Heat transfer during condensation of HFC 134a and R404a inside of a horizontal smooth and micro-fin tube, *Experimental Thermal Fluid Science,* Vol. 34, 2010, pp. 1133–1141.

[13] Lyulin, Y., Marchuk, I., Chikov, S. and Kabov, O., Experimental study of laminar convective condensation of pure vapour inside an inclined circular tube, *Microgravity Science Technology,* Vol. 23, 2011, pp. 439 - 445.

[14] REFPROP, NIST Thermodynamic Properties of Refrigerants and Refrigerant Mixtures (REFPROP), version 8.0, NIST Standard Reference Database 23, National Institute of Standards and Technology, Gaithersbury, MD, 2005..

[15] Bhagwat, S.M. and Ghajar, A. J., A flow pattern independent drift flow model based void fraction correlation for a wide range of gas-liquid two-phase flow, *International Journal of Multiphase Flow,* Vol. 59, 2014, pp. 188-205.

EFFECT OF A SHARP RETURN BEND ON TWO-PHASE REFRIGERANT FLOW VOID FRACTION

De Kerpel K.*, De Schampheleire S., and De Paepe M.
*Author for correspondence
Department of Flow, Heat and Combustion Mechanics,
Ghent University - UGent,
Ghent, 9000,
Belgium,
E-mail: Kathleen.DeKerpel@ugent.be

ABSTRACT

In this work, the void fraction is measured for two-phase refrigerant flow at several locations up-and downstream of a sharp return bend. The tube diameter D ranges between 4.83 mm and 8 mm and the curvature radius of the bend (2R/D) ranges between 2.5 and 4.5. The void fraction measurement is based on the electrical capacitance of the flow. The refrigerant used is R134a, the mass flux was varied between 200 and 600 kg/m²s and the vapour quality varied between 0 and 1. The tubes up-and downstream of the return bend are horizontal and the plane of the bend is placed vertical. Downward as well as upward oriented flow through the bend was tested. Three flow regimes were observed: slug flow, intermittent flow and annular flow. A significant effect is observed downstream of the return bend, upstream the result was limited. Furthermore, the influence of the bend decreases with decreasing channel diameter.

INTRODUCTION

Compact fin-and-tube heat exchangers are used in a wide range of applications, one example being air-source heat pumps. In such heat exchangers, the tube is folded up into a sequence of sharp 180° bends and straight sections, in order to attain a high compactness.

The presence of these bends has an influence on the flow behaviour up- and downstream of these bends. In case of two-phase flow, the difference between the properties of the phases can lead to a significant distortion of the phase distribution in and in the vicinity of the bend. Since there is a strong link between the flow behaviour and the pressure drop and heat transfer in the heat exchanger, it is important to gain more insight in the link between the bend geometry and the intensity and extent of the disturbance of the flow behaviour. This will lead to better design methods for compact heat exchangers for domestic applications.

In this work, the void fraction is measured at several locations up- and downstream of a sharp return bend. Three different bend geometries are tested, two of which have a channel diameter of 8 mm and one with a channel diameter of 4.83 mm. The void fraction is measured by means of a capacitance sensor.

NOMENCLATURE

D	[m]	channel diameter
G	[kg/m²s]	mass flux
R	[m]	bend radius
S	[-]	velocity ratio
T	[K]	temperature
V	[m/s]	velocity
x	[-]	vapour quality
ε	[-]	void fraction
ρ	[kg/m³]	density

TEST SETUP

The test section used in this work consists of a sharp return bend interconnecting two horizontal straight channels. The bend plane is placed vertical and both upward oriented and downward oriented flow through the bend are tested. Three different return bends geometries are tested: one with D = 8 mm and R = 11 mm (2R/D = 2.75), one with D = 8 mm and R = 15.8 mm (2R/D = 3.95) and one with D = 4.83 mm and R = 7.8 mm (2R/D = 3.22).

The void fraction is measured through a capacitance sensor. Due to the difference in dielectric constant between the liquid and vapour phase, the capacitance of the flow depends on the amount of each phase present and can be linked to the void fraction. The link between the measured capacitance and the void fraction is non-linear and dependent on the two-phase flow regime, the calibration technique proposed by De Kerpel et al. [1, 2] is used. As shown in Figure 1, this capacitance is measured between two concave electrodes, each with an angle of 160°. To attain a good spatial resolution, the axial length of the electrodes is limited to one tube diameter.

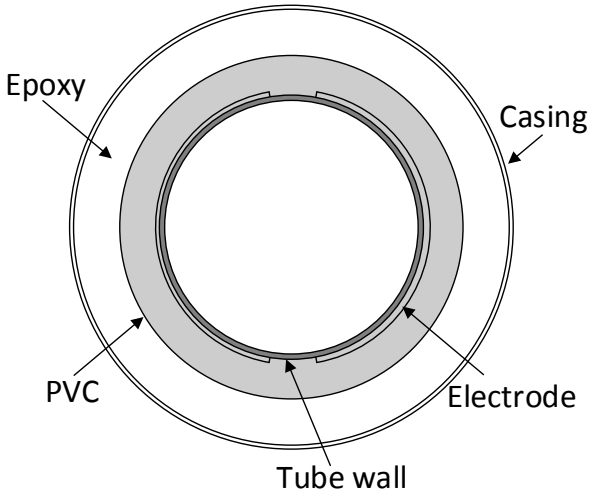

Figure 1 Cross section of capacitance sensor

The void fraction is measured at several locations up- and downstream of the return bend, these locations are indicated by the distance between the bend inlet and the sensor for locations upstream of the return bend and as the distance between the bend outlet and the bend for locations downstream of the return bend. These distances are expressed as a number of tube diameters D and are negative for upstream positions, e.g. the sensor at location 2.5D for a bend with channel diameter 8 mm is located at 20 mm downstream of the return bend outlet. For each geometry and flow direction, the void fraction is measured at a location far upstream of the bend, where the bend effect is assumed to be non-existent [3, 4] and the void fraction measured at this location will be taken as a reference. Downstream of the return bend, the void fraction is measured at 2.5D, 8.5D, 34.5D and 85D. The refrigerant used is R134a, the mass flux was varied between 200 and 500 kg/m²s and the vapour quality varied between 0 and 1. Two saturation temperatures are tested: 10°C and 15°C. Three flow regimes were observed: slug flow, intermittent flow and annular flow.

MEASUREMENTS AND DISCUSSION

In this section, the measured void fractions at different locations are discussed for each bend geometry and flow direction. The first part of this section deals with the results for downward oriented flow (gravity assisted flow) and the second part deals with upward oriented flow (gravity opposed flow).

Downward oriented flow

Figure 1 shows the measured void fraction for downward flow as a function of vapour quality for the different mass fluxes at T = 15°C for a return bend with R = 11 mm and D = 8 mm. For the sake of simplicity, the results for T = 10°C are not shown here, but the conclusions are the same. Figure 1 shows an increase in void fraction for vapour qualities ranging from 10% to 50% for the sensor locations 2.5D, 8.5D and 34.5D. Further downstream, at 85D, the void fraction coincides with the reference value at -34.5D.

$$\varepsilon = \frac{\frac{x}{\rho_V}}{\frac{x}{\rho_V} + S\frac{1-x}{\rho_L}} \quad (1)$$

Based on the definition of the vapour quality and the void fraction, the void fraction can be written as shown in Eq. (1), in this equation S is the ratio of the vapour phase velocity V_v to the liquid phase velocity V_L [5]. If the void fraction increases for a constant vapour quality and constant density of the phases, the velocity ratio S should decrease. Hence, an increase in void fraction indicates that the liquid phase velocity increases relative to the vapour phase velocity. This observation is consistent with the results found for air-water two-phase flow through a return bend [6]. It was found that in the bend, a separation of the phases occurs in which the liquid phase is pushed to the outer wall of the bend. This is a result of the difference in centrifugal force applied to the phases in the return bend due to their difference in density. Due to this phase separation, the liquid phase velocity is temporarily increased relative to the vapour phase velocity. This acceleration is reflected in the void fraction measurements for a return bend with R = 11 mm and D = 8 mm.

Figure 3 shows the void fraction measurements for a bend with R = 15.8 mm and D = 8 mm. Again, no significant difference is observed between the void fraction measured far downstream of the bend (85D) and the reference measurement far upstream. For the measurement closest downstream of the return bend, at 2.5D, an increase in void fraction compared to the reference measurement is again observed. However, further downstream at 8.5D and 34.5D, this acceleration is absent for G = 200 kg/m²s and G = 300 kg/m²s. For higher mass fluxes, the void fraction at 8.5D does show an increase compared to the reference, however, the void fraction at 34.5D does not differ significantly from the reference. The difference between Figure 2 and Figure 3 can be explained by the difference in the bend radius between both bend geometries. The bend associated with Figure 3 has a larger curvature ratio than the one associated with Figure 2. Since the centrifugal force is inversely proportional to the radius of curvature, the separation of the phases will be less intense for the bend with the larger radius. Hence the bend disturbance of the flow due to the bend will dissolve over a shorter distance downstream of the return bend, compared to the bend with the smaller radius. On the other hand, the centrifugal force is also proportional to the velocity of the phases. As the mass flux increases, the velocity of the phases will rise as well for a constant vapour quality and tube diameter. This explains the increase in void fraction at 8.5D (and 34.5D) with increasing mass flux.

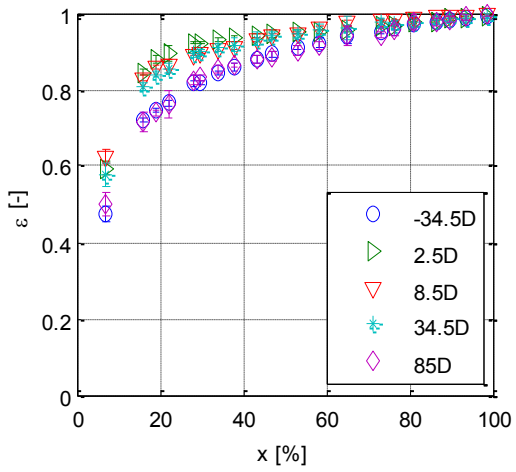

a) G = 200 kg/m²s

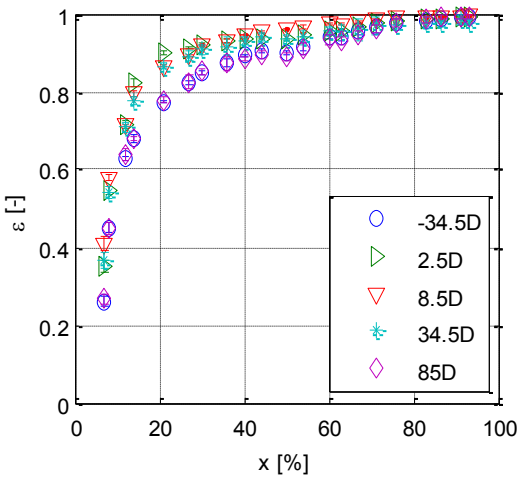

b) G = 300 kg/m²s

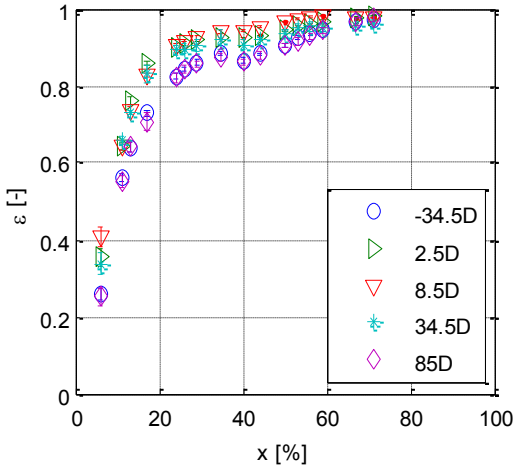

c) G = 400 kg/m²s

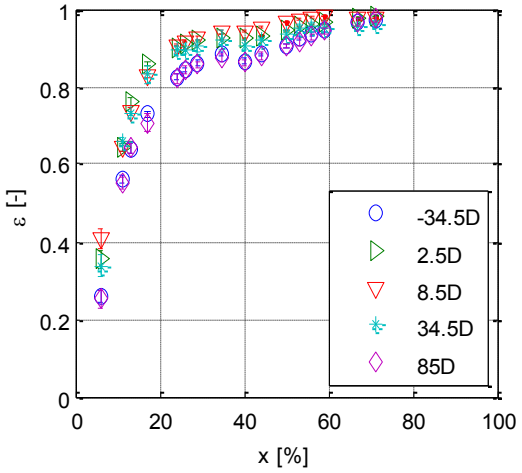

d) G = 500 kg/m²s

Figure 1: R = 11 mm and D = 8 mm, downward oriented flow

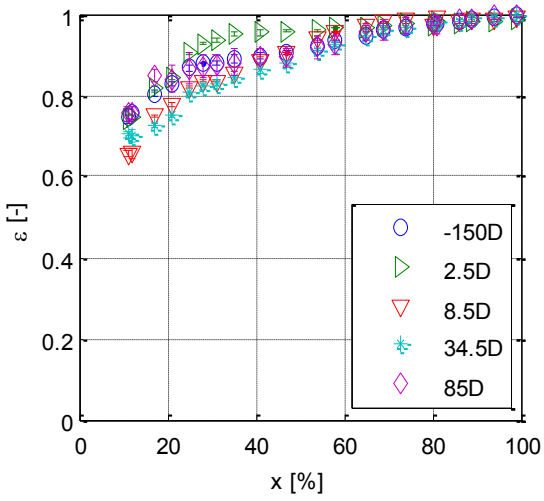

a) G = 200 kg/m²s

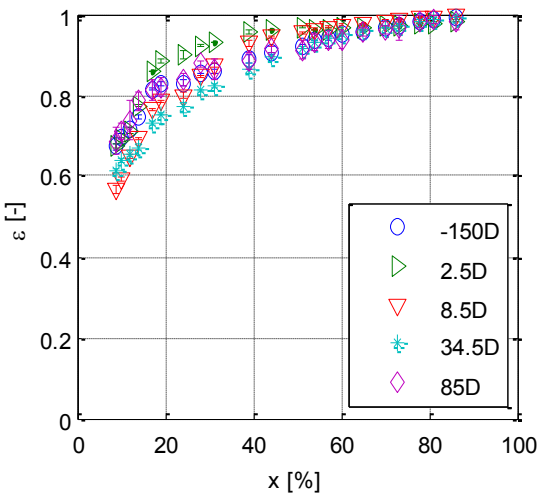

b) G = 300 kg/m²s

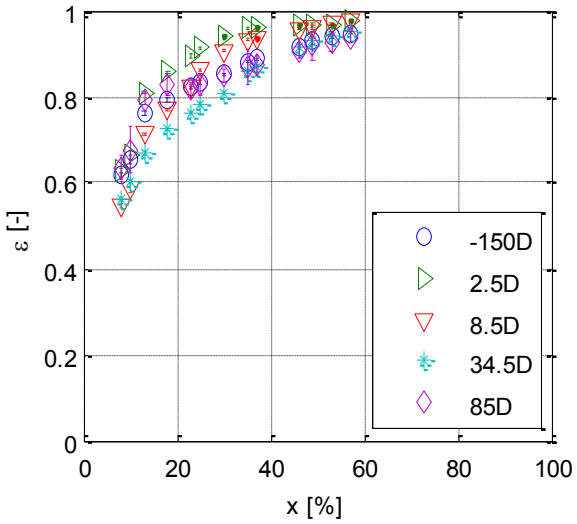

c) G = 400 kg/m²s

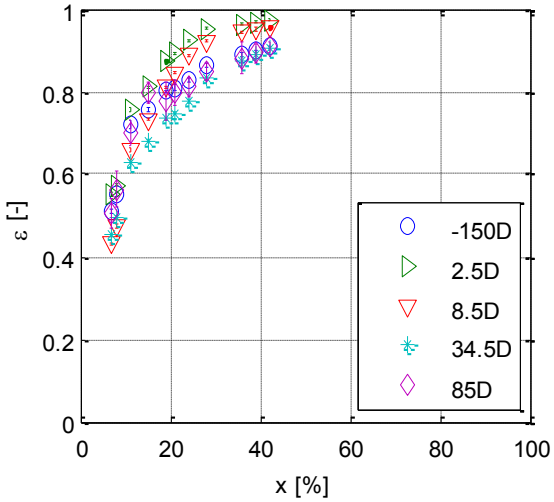

d) G = 500 kg/m²s

Figure 3: R = 15.8 mm and D = 8 mm, downward oriented flow

Figure 4 shows the result for a bend with the smaller channel diameter. For the sake of simplicity, the results for G = 500 kg/m²s are not shown; however, the conclusions remain the same. Although the curvature ratio of this bend 2R/D = 3.22 is an intermediate value between the two other tested bend ratios, no significant difference between the void fraction measurements at different locations are observed for downward oriented flow. This is a consequence of the smaller channel diameter. As the channel diameter reduces, the effect of the surface tension increases relative to the effect of gravity and centrifugal force [7]. However, it should be noted that the lowest vapour quality shown in Figure 4 is 20% and any bend effect occurring at lower void fractions cannot be excluded.

Upward oriented flow

Figure 5 shows the measured void fraction for the bend with R = 11 mm and D = 8 mm for upward oriented flow. Again, the measurement far downstream of the return bend, at 85D, matches the reference measurement well. A slight decrease in void fraction compared to the reference is seen at locations 2.5D, 8.5D and 34.5D. This is the most pronounced at low mass fluxes. For upward oriented flow the liquid phase is also pushed to the outside wall of the bend. However, for this orientation, the liquid

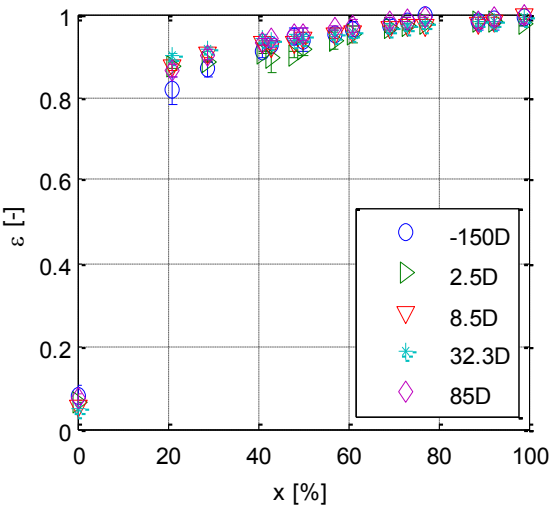

a) G = 300kg/m²s

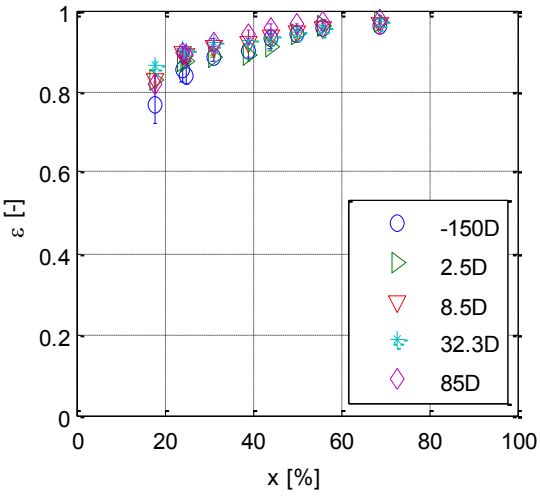

b) 400 kg/m²s

Figure 2 : R = 7.8 mm and D = 4.83 mm, downward oriented flow

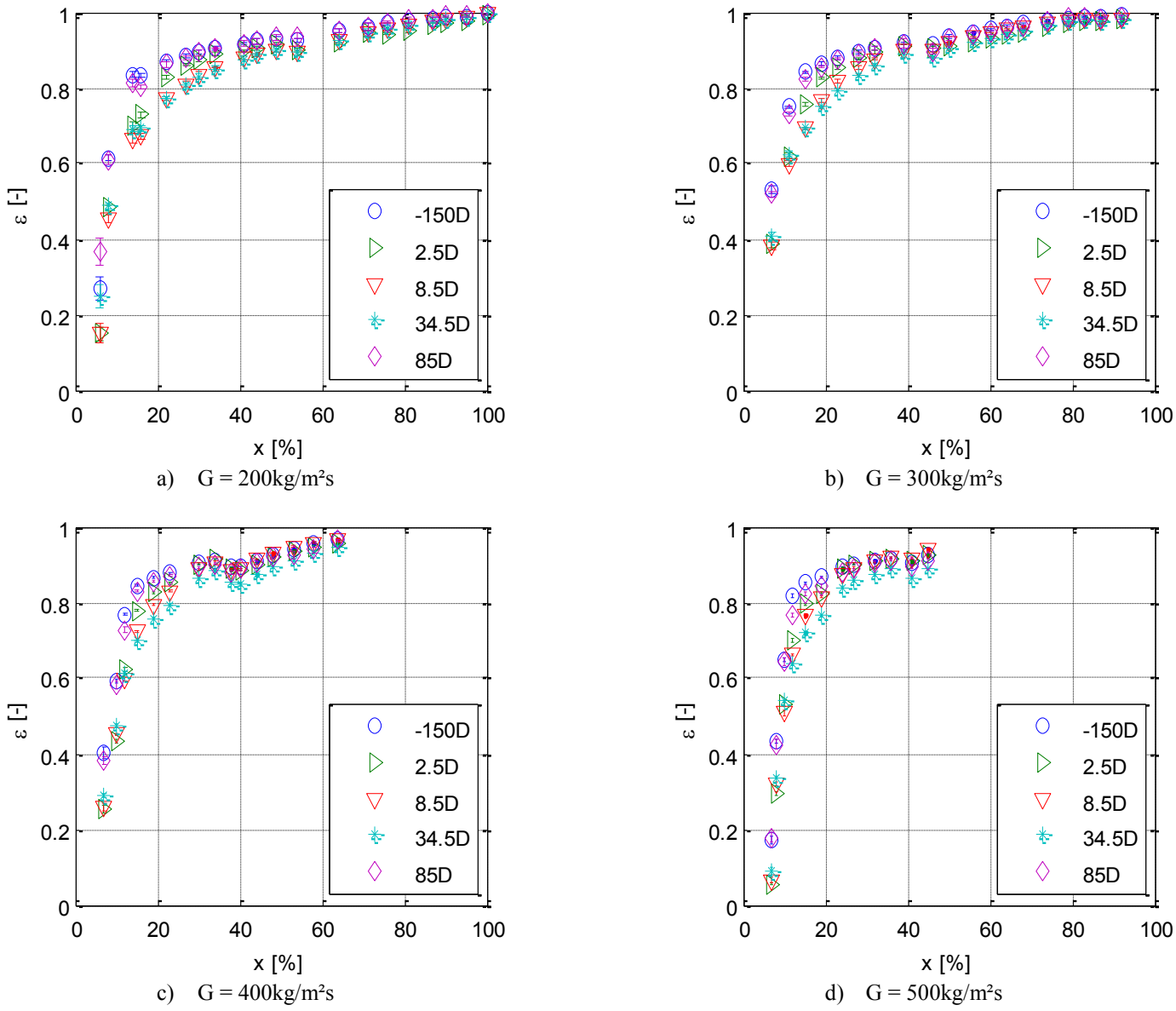

Figure 4: R = 11 mm and D = 8 mm, upward oriented flow

phase is located at the top of the tube at the outlet of the return bend. Due to the action of gravity, which pulls the liquid layer down from the top of the tube, the remixing of the phases occurs more acutely compared to the downward oriented case. The observed decrease in void fraction is most likely due to the reduction of the velocity in the axial direction of the liquid phase due to the action of gravity.

In Figure 5 the void fraction for R = 15.8 mm and D = 8 mm for upward flow are shown. For the sake of simplicity, the results for G = 300 kg/m²s and G = 500 kg/m² are not shown; however, the conclusions are the same for all mass fluxes. Figure 5 shows a slight increase in void fraction for the locations 2.5D, 8.5D and 34.5D. However, this increase is only significant at high mass fluxes and vapour qualities. Despite the limited significance of this acceleration, it is quite different from the case shown in Figure 4, where a slight decrease in void fraction was observed. For air-water flow an increase in the void fraction close downstream of a return bend for both the upward and downward oriented case has been reported in literature [8]. The return bend used by de Oliveira et al. had a relatively high curvature ratio of 8.7.

The fact that the sharper return bend causes a decrease in void fraction close to the bend outlet can be explained by the higher centrifugal force acting on the flow in the return bend. This leads to a stronger separation of the phases in the bend and hence a thicker liquid layer at the top of the channel at the bend outlet. As a consequence, the remixing under the action of gravity will be more intense, counteracting the acceleration of the liquid phase in the bend.

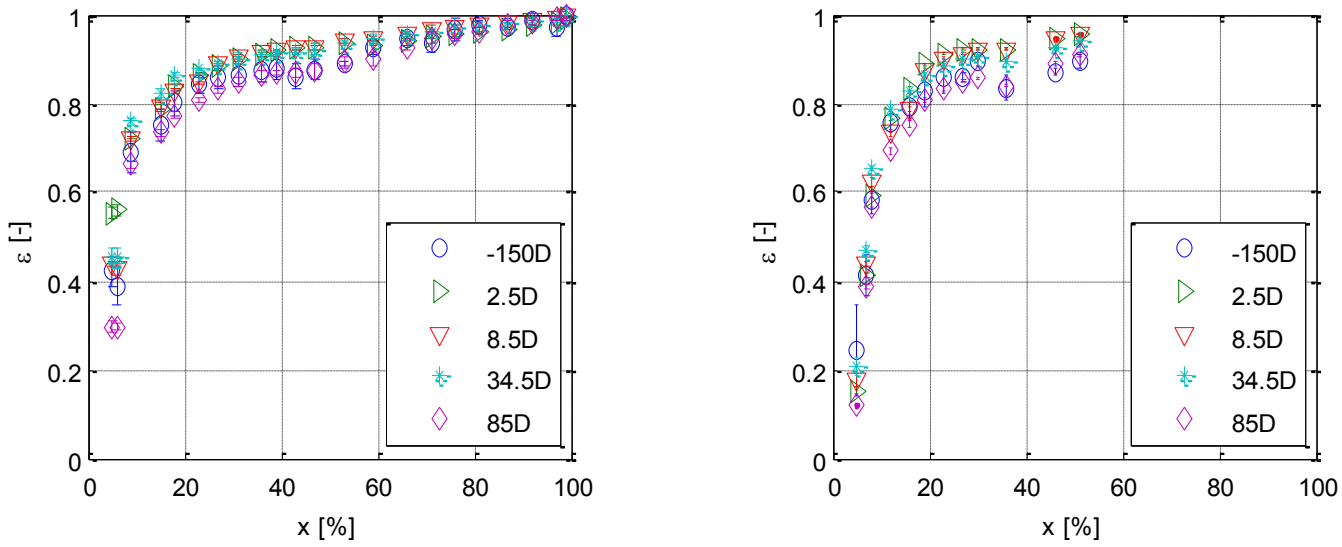

a) 300 kg/m²s b) 400 kg/m²s

Figure 5: R = 15.8 mm and D = 8 mm, upward oriented flow

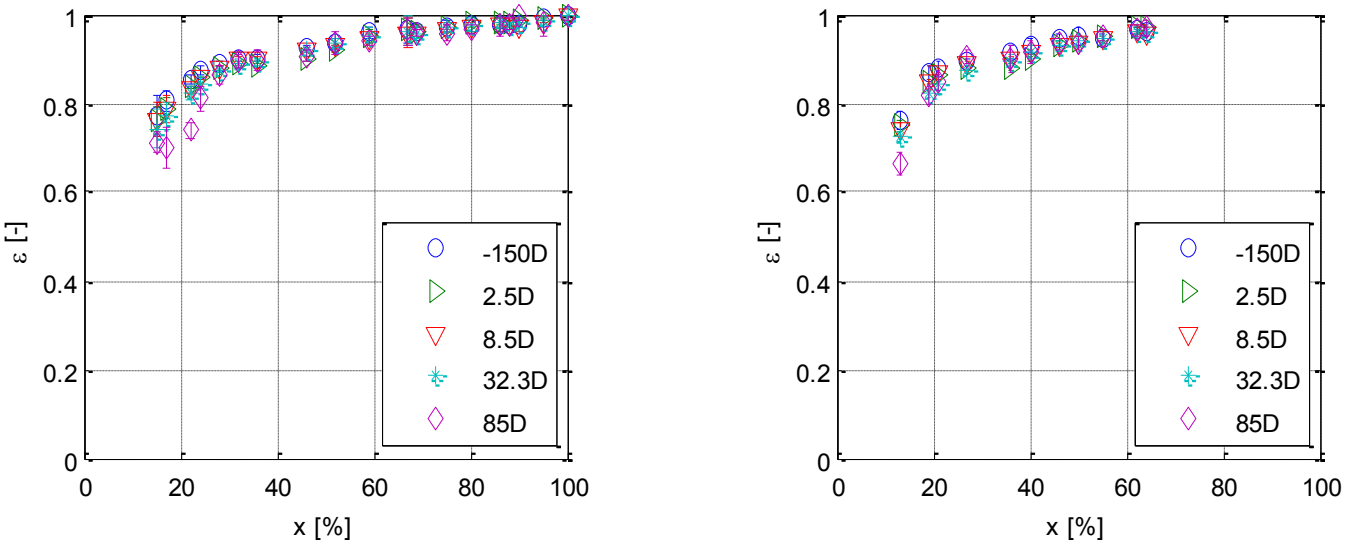

a) 300 kg/m²s b) 400 kg/m²s

Figure 6: R = 7.8 mm and D = 4.83 mm, downward oriented flow

Figure 7 shows the void fraction measured for the bend with 7.8 mm and D = 4.83 mm in upward oriented flow. As was the case for downward oriented flow, no significant effect on the void fraction due to the return bend is observed. This is a result of the greater relative influence of the surface tension compared to gravity and centrifugal forces [7].

CONCLUSIONS

In this work the effect of a sharp return bend on the two-phase flow void fraction close up- and downstream is investigated. The void fraction is measured with a capacitance sensor.

For downward oriented flow, an increase in void fraction is observed for the bends with a channel diameter of 8 mm. This increase was seen to persist up to 34.5D downstream for the bend with the lowest radius (11 mm) while for the bend with the higher radius (15.8 mm) the increase in void fraction was only observed until 15.8 mm downstream of the bend outlet. For the bend with the smaller channel diameter (D = 4.83 mm) no effect of the return bend was observed in the void fractions, this is due to the larger relative importance of the surface tension.

For upward oriented flow through the return bend, again an increase in void fraction is observed for the bend with R = 15.8 mm and D = 8 mm. However, this increase is only very limited. Furthermore, the bend with the same channel diameter and a lower bend radius shows a decrease in void fraction. This can be explained by a more intense remixing of the phases at the outlet

of the bend. Finally, the bend with the smaller channel diameter does not show a significant effect on the void fraction due to the return bend.

ACKNOWLEDGEMENTS

This research was funded with a PhD grant (nr. 111192) of the Agency for Innovation by Science and Technology (IWT).

REFERENCES

[1] De Kerpel, K., Ameel, B., T'Joen, C., Canière, H., De Paepe, M., Flow regime based calibration of a capacitive void fraction sensor for small diameter tubes, *International Journal of Refrigeration,* Vol. 36(2), 2013, pp. 390-401.

[2] De Kerpel, K., Ameel, B., De Schampheleire, S., T'Joen, C., Canière, H., De Paepe, M., Calibration of a capacitive void fraction sensor for small diameter tubes based on capacitive signal features, *Applied Thermal Engineering,* Vol. 63(1), 2014a, pp. 77-83.

[3] De Kerpel, K., De Keulenaer, T., De Schampheleire, S., De Paepe, M., Capacitance sensor measurements of upward and downward two-phase flow in vertical return bends, *International Journal of Multiphase Flow,* Vol. 64, 2014b, pp. 1-10.

[4] Da Silva Lima, R., Experimental and Visual Study on Flow Patterns and Pressure Drops in U-Tubes, PhD Thesis, *LTCM,* Ecole Polytechnique Fédérale de Lausanne, Lausanne, Switzerland, 2011

[5] Collier, J., Thome, J., 1994, *Convective Boiling and Condensation*, Oxford Science Publications, Oxford, United Kingdom.

[6] Wang, C.-C., Chen, I. Y., Lin, Y.-T., Chang, Y.-J., A visual observation of the air-water two-phase flow in small diameter tubes subject to the influence of vertical return bends, *Chemical Engineering Research & Design*, Vol. 86(11A), 2008, pp. 1223-1235.

[7] Wang, C.-C., Chen, I. Y., Chang, Y.-J., Two-phase flow pattern in small diameter tubes with the presence of horizontal return bend, *International Journal of Heat and Mass Transfer*, Vol. 46(16), 2003, pp. 2975-2981.

[8] de Oliveira, P., Strle, E., Barbosa Jr., J., Developing air–water flow downstream of a vertical 180° return bend, *International Journal of Multiphase Flow*, Vol. 67(0), 2014, pp. 32-41.

A STUDY OF HEAT EXCHANGE THROUGH AN HELICO-AXIAL ROTOR OF A MULTIPHASE PUMP

Pagnier Ph.* and Teixeira D.
*Author for correspondence
Fluid Mechanics Department,
Applied Mechanics Division,
IFP Energies nouvelles,
Solaize 69360,
France,
E-mail"philippe.pagnier@ifpen.fr"

Ekeberg I. and Torkildsen B.H.
Pumps and Subsea Process Systems,
Processing Systems,
OneSubsea,
Sandsli 5254,
Norway,

ABSTRACT

The present paper deals with the investigations carried out by IFP Energies nouvelles and OneSubsea within a collaboration, aiming at getting a better understanding of the internal flows and heat exchange between gas and liquid flowing through an axial rotodynamic multiphase pump. This kind of pumps is now largely used in petroleum industry, especially for subsea applications, to carry oil, water and gas economically in a single pipe. The technology is used increasingly at oil fields and consists in a multi-stage helico-axial pump, where each stage is composed of a stator and a rotor which resembles an inducer. Number of studies are aimed at modeling the behavior of this kind of pumps in single phase [1], [2], or in two-phase flows for centrifugal pumps [3], [4], [5].

The assessment of the temperature elevation at the outlet of each stage of the multiphase pump becomes a challenge for the pump suppliers who want to select the optimized solution faced to the operating conditions of a given field. When a rotodynamic machine pumps a mixture of gas and liquid, degradations of performance (i.e. pressure gain and efficiency versus flow rate) are commonly observed depending on the gas volume fraction (GVF), especially for centrifugal pumps and to a lesser extend for axial pumps. The degradation of the pressure gain when GVF increases, is related to an elevation of the temperature which impacts both the viscosity and the specific gravity of the mixture.

The objective of the study detailed in the present paper is describing the heat exchange models used to compute the temperature elevation through an axial compression cell of a pump. Two models are suggested: the first one is a simple model developed with the main assumption of an homogeneous mixture. The second one is based on a two-fluid model which is more representative of the realistic phenomena that occur in such of axial cells. The models are discussed and the results are compared to the global experimental data supplied by OneSubsea. In the end of the project currently in progress, the thermal model will be implemented in a global zero-D software capable to predict the performances of a multiphase pump.

INTRODUCTION

Multiphase compression units (so called MPP for Multi Phase Pump) for the compression of mixtures made with natural gas and crude oil, are now widely used in the oil domain to enhance the well's recovery rate. The rotodynamic axial pump technology – so-called Poséidon, developed by IFP Energies nouvelles in the 1990s – constitutes an attractive way that meets the oil company's needs for subsea or topside/onshore applications. OneSubsea is the leading supplier of subsea solutions including MPP.

The compression stations have to be more and more powerful and capable of meeting a large variability of the operating conditions depending on the well's life. Thus, OneSubsea is led to design booster machines with the widest range of total flow rate, gas volume fraction and viscosity (up to 4000 cP). With that goal, the mixture's temperature elevation at the entry of each stage of a multiphase pump constitutes a crucial data for the predictive computation of the global performances of an MPP operated with viscous crude oil.

NOMENCLATURE

GVF	[%]	Gas Volume Fraction noted α
$\delta\omega$	[J/kg]	Elementary work
dP	[Pa]	Pressure gain
δq	[J/kg]	Elementary heat transfer
u	[J/kg]	Internal energy
dV	[m^3]	Element of volume
dh	[J/kg]	Variation of Enthalpy
du	[J/kg]	Variation of internal energy
dT	[K]	Temperature elevation
dS	[J/kg]	Variation of Entropy
Cp	[J/kg/K]	Heat Capacity
q	[m^3/s]	Flow rate
W	[W]	Exchange of Work
Q	[W]	Exchange of Heat
Rb	[m]	Bubble radius
L	[m]	Axial Length of a stage
S	[m²]	Cross Section of a stage
x_g	[-]	Gas Mass Fraction
k	[-]	Polytropic Coefficient
P	[Pa]	Pressure
T	[K]	Temperature
α_{poly}	[-]	Coefficient of proportionality

Special characters

α	[%]	Gas Volume Fraction
ρ	[kg/m^3]	Specific gravity
η	[%]	Efficiency
γ	[-]	Laplace Coefficient
ς	[-]	Isentropic Coefficient
θ	[-]	Partial Heat Exchange

Subscripts

i	Input work
c	Kinetic energy
loss	Dissipated heat due to stress along the walls
ext	Heat exchange with external
liq	Liquid
gas	Gas
t	Total
2φ	Two-phase mixture
f2	Final temperature at the outlet
1	Inlet of a stage
2	Outlet of a stage

In the frame work of a close collaboration, IFP Energies nouvelles and OneSubsea have developed thermal models to be implemented in an in-house processing software capable of predicting the performance (i.e. pressure gain, temperature elevation and shaft power versus total flow rate for a given rotation speed and for a given gas volume fraction) of any MPP configuration at field specific operating conditions. The first thermal model consists in the equations used for enthalpy variations of an homogeneous mixture while the second model deals with the heat exchanges that occur between the two phases of the mixture during the compression of the flow through a stage.

The present paper focuses on the development of these two thermal models. Then the models are used separately for a predictive computation of the performances of an MPP and finally compared with the global experimental data.

THERMAL MODELS

When an MPP is operated at a very low GVF, the compression of a gas / liquid mixture could be assumed to be isothermal: the heating of gas by compression and the heating by power losses could be neglected. As gas is cooled down by liquid, this assumption is relatively acceptable as long as GVF is lower than 20 or 25 %, or as long as the compression pressure ratio is moderate. Even though the isothermal assumption could be acceptable to predict the global performances of an MPP using the assumption given above, the temperature elevation is useful for design purposes. In addition, manufacturers are led to design more powerful MPPs for wider operating ranges. Therefore, the basic isothermal assumption becomes obsolete and the development of a more realistic model is required to reproduce heat exchanges between gas and liquid and finally to predict the temperature rises with an acceptable accuracy.

Two thermal models have been developed by IFP Energies nouvelles within the framework of a collaboration with OneSubsea. The main assumption used for both the two models are given below:

- The mixture is heated by the hydraulic power losses and by the compression through the pump;
- Gas is cooled down by liquid;
- Gas is assumed to be an ideal gas in a first step. This assumption is sufficient for now for an industrial application but could be extended to real gas afterward for next developments;
- The thermal steady state is reached with the casing and the different components of the pumps.

Model of homogenous mixture

The first approach in the development of an accurate and realistic model of heat exchange consists in considering the mixture as an ideal homogeneous mixture through a compression stage. Thus, additional conditions have to be assumed comparing with the main assumptions given above:

- Phases are in a thermal equilibrium (i.e. same temperature of gas and liquid through the stage);
- The mixture is totally homogeneous meaning that gas and liquid occupy the volume of a stage in the same manner and that no slippage exists between the two phases.

Consequently, the elementary works transferred through the rotor of the compression stage can be written as follows:

$$\delta\omega_i = \delta\omega_c + \frac{dP}{\rho} + \delta q_{loss} \quad (1)$$

In addition, the variation of the total internal energy can be written with the expression (2):

$$du = \delta q_{ext} - PdV + \delta q_{loss} \quad (2)$$

Combining (1) and (2), and introducing the enthalpy variation dh:

$$dh = \delta q_{loss} + \delta q_{ext} + \frac{dP}{\rho} \quad (3)$$

or

$$dh + d\omega_c = \delta\omega_i + \delta q_{ext} \quad (4)$$

The relation (4) simply means that the supply of mechanic elementary energy and external heat leads to a variation of the total enthalpy of fluid.

Neglecting the coefficient of thermal isobaric expansion for liquid and using the Gay-Lussac law for an ideal gas, the enthalpy variation for liquid and gas is expressed with relationships (5) and (6) respectively:

$$dh_{liq} = Cp_{liq}dT + \frac{dP}{\rho_{liq}} \quad (5)$$

$$dh_{gas} = Cp_{gas}dT \quad (6)$$

Finally, the variation of enthalpy for each phase can be expressed in terms of energy with the assumption of kinetic energy conservation between the entry and outlet of a stage:

$$\rho_{liq} q_{liq} dh_{liq} = dW_{i-liq} + dQ_{ext-liq/gas} \quad (7)$$

$$\rho_{gas} q_{gas} dh_{gas} = dW_{i-gas} + dQ_{ext-gas/liq} \quad (8)$$

Combining (5) to (8) and using (1), the variation of enthalpy of the mixture leads to the equation (9) for the assessment of the temperature rise.

$$\left(\rho_{liq} q_{liq} Cp_{liq} + \rho_{gas} q_{gas} Cp_{gas}\right) dT = dQ_{loss} + q_{gas} dP \quad (9)$$

In (9), the heat quantity received by liquid is assumed to be the opposite of the heat quantity left by gas:

$$dQ_{ext-gas/liq} = -dQ_{ext-liq/gas} \quad (10)$$

In addition, the total work supplied on the shaft W_t can be broken down in the total losses Q_{loss} dissipated to heat, and the work received by fluids $W_{i,t}$ which represents the sum of the work received by gas and the work received by liquid. Therefore, introducing the efficiency of the compression, the global losses dissipated to heat can be expressed as below:

$$dQ_{loss} = dW_{i,t}\left(\frac{1-\eta_{2\varphi}}{\eta_{2\varphi}}\right) \quad (11)$$

Thus the equation (9) derives into the following expression:

$$\left(\rho_{liq} q_{liq} Cp_{liq} + \rho_{gas} q_{gas} Cp_{gas}\right) dT = dW_{i,liq} \frac{1-\eta_{2\varphi}}{\eta_{2\varphi}} + dW_{i,gas} \frac{1}{\eta_{2\varphi}} \quad (12)$$

Introducing the Mayer's relationships for an ideal gas and the gas mass fraction x_g defined as follows:

$$x_g = \frac{\rho_{gas} q_{gas}}{\rho_{gas} q_{gas} + \rho_{liq} q_{liq}} \quad (13)$$

and introducing the isentropic coefficient ζ with the expression

$$\zeta = \frac{(1-x_g) Cp_{liq} + x_g Cp_{gas}}{(1-x_g) Cp_{liq} + x_g Cv_{gas}} \quad (14)$$

and the polytropic coefficient n defined as:

$$\frac{n}{n-1} = \frac{1}{\eta_{2\varphi}} \frac{\zeta}{\zeta - 1} \quad (15)$$

the final equation used to assess the temperature rise of the mixture can be described with the relationship (16) using (12):

$$\frac{dT}{dP} - \left(\frac{1-n}{n}\right)\frac{T}{P} = \frac{1-\eta_{2\varphi}}{\eta_{2\varphi}} \frac{1-x_g}{(1-x_g) Cp_{liq} + x_g Cp_{gas}} \frac{1}{\rho_{liq}} \quad (16)$$

The equation (16) can be solved easily and derived to the following expression:

$$T_2 = T_1\left(\frac{P_2}{P_1}\right)^{\frac{n-1}{n}} + \left(\frac{1-\eta_{2\varphi}}{\eta_{2\varphi}}\right) \frac{1-x_g}{(1-x_g) Cp_{liq} + x_g Cp_{gas}} \left(\frac{P_2 - P_1}{\rho_{liq}}\right) \quad (17)$$

The final equation of the temperature at the outlet of a stage depends on the fluids properties, the efficiency of the gas - liquid mixture compression, the GVF and of course on the pressure elevation through the stage in two-phase flow. The performances of a multiphase pump in terms of pressure gain and efficiency, whether an axial pump or a centrifugal one have been studied and modelled by number of authors. For instance Furuya O [6] developed an analytical model to predict the performances of a mixed flow pump operated with a mixture of air and water within a completed range of GVF from 0 to 1. Gülich J.F. [4] detailed the effects of the presence of gas on the performances of a multistage axial pump and used a two-phase multiplier for the computation of the pressure gain. For the present study, the authors have developed a proprietary tool capable of computing the shaft power and pressure gain as function of the flow rate for a given rotation speed and a given GVF. The method is not detailed in the present paper.

Two-fluid model

With this model, the following process is considered:

- Liquid and gas are compressed separately without any exchange leading to different temperature elevations for gas and liquid;
- Then liquid and gas exchange heat quantity totally to reach a final equivalent temperature of the mixture.

Therefore, in one hand, the compression of liquid leads to the temperature elevation dT_{liq}, using (5), (7) and (11).

$$dT_{liq} = \frac{dP}{\rho_{liq} Cp_{liq}} \frac{1-\eta_{liq}}{\eta_{liq}} \quad (18)$$

and finally to the temperature of liquid at the outlet of the stage T_{liq2} is given by the equation (19):

$$T_{liq2} = T_{liq1} + \frac{1}{\rho_{liq} Cp_{liq}}\left(\frac{1-\eta_{liq}}{\eta_{liq}}\right)\left(P_2 - P_1\right) \quad (19)$$

In other hand, the compression of gas is assumed to be polytropic. Thus, the variation of gas enthalpy is proportional to the variation of entropy using the coefficient of proportionality α_{poly}.

$$TdS = \delta q_{extG/L} + \delta q_{frot} = \alpha_{poly} dh \quad (20)$$

Therefore the well-known equation for a polytropic gas compression can be used:

$$\frac{k}{k-1}\frac{dT}{T}=\frac{dP}{P} \tag{21}$$

where the coefficient k represents the polytropic coefficient

$$\frac{k}{k-1}=\left(1-\alpha_{poly}\right)\frac{\gamma}{\gamma-1} \tag{22}$$

Then, the equation (21) leads to the assessment of the gas temperature at the outlet of the stage using the well-known equation (23).

$$T_{gas2}=T_{gas1}\left(\frac{P_2}{P_1}\right)^{\frac{k-1}{k}} \tag{23}$$

The coefficient of proportionality α_{poly} can be defined using (22) as follows:

$$\alpha_{poly}=1-\left(\frac{k}{k-1}\right)\left(\frac{\gamma-1}{\gamma}\right) \tag{24}$$

with (25) using (6), (8) and (11)

$$\frac{k-1}{k}=\frac{1}{\eta_{gas}}\left(\frac{\gamma-1}{\gamma}\right) \tag{25}$$

Assuming the residence time is sufficient for heat exchange to be completed, the final equivalent temperature of the mixture reaches the value T_{f2} given by the equation (26).

$$T_{f2}=\frac{\rho_{liq}q_{liq}c_{Pliq}T_{liq2}+\rho_{gas}q_{gas}c_{Pgas}T_{gas2}}{\rho_{liq}q_{liq}c_{Pliq}+\rho_{gas}q_{gas}c_{Pgas}} \tag{26}$$

or also (27), using (13)

$$T_{f2}=\frac{\left(1-x_g\right)c_{Pliq}T_{liq2}+x_g c_{Pgas}T_{gas2}}{\left(1-x_g\right)c_{Pliq}+x_g c_{Pgas}} \tag{27}$$

Discussion on the two models

The first model detailed in the present document assumes that an homogeneous mixture exists spatially through a compression stage. This implies a non-slippage condition between gas and liquid. Moreover, gas and liquid are assumed to be in thermal equilibrium in a steady state. Therefore, the heat transfer between gas and liquid is assumed to be a completed exchange and the overall losses due to frictions between the two phases are included in the two-phase efficiency $\eta_{2\varphi}$. Obviously, a type of flow such as dispersed flow with internal forces is not taken into account with this model.

The second model is much more detailed than the first one as it includes thermal unbalance. Due to the compressibility of gas, its temperature rise can be much higher than the temperature elevation of liquid, depending on the pressure gain of the compression stage and the GVF. Thus, the model introduces the efficiency of the compression for each phase which could be different considering the viscous effects and the drag forces. In addition, the slippage between gas and liquid could be introduced in this model leading to a forced convection heat exchange between the two phases.

To illustrate the use of the model, an basic example is presented for a six-stage pump operated with air and water. Parameters are detailed in the Table 1.

Designation	Value	Unit
η	60	%
GVF	70	%
T_1	313	K
P_1	1	bar
dP per stage	1	bar

Table 1: Parameters for a six-stage pump

For this specific example, the computation is performed stage by stage, assuming a constant efficiency for the compression through each stage, even if GVF is not constant. In the next section, the thermal models are used computing values of efficiency in two-phase flows, stage by stage by means of an in-house software.

The Figure 1 shows the variation of the temperature at the outlet of each stage for gas and liquid using the two-fluid model. This figure also shows the equivalent temperature of the mixture assuming a completed heat transfer between the two phases using (26).

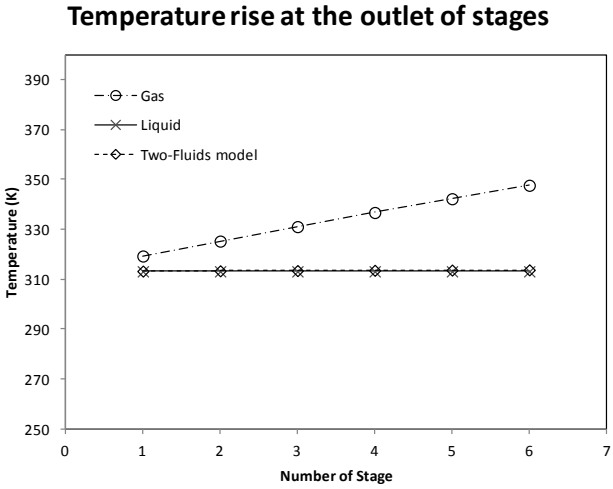

Figure 1 Variation of temperature through a multistage pump

Although the gas temperature rise is higher than the temperature rise of the liquid, the final temperature of the mixture is close to the liquid one, even for a GVF of 70 %. This

result can be explained by the effects of very low mass gas fraction in the equation (27).

Using identical operating conditions, temperature rise obtained using the homogeneous and the two-fluid models are both presented in Figure 2. The figure shows a slight discrepancy between the two models.

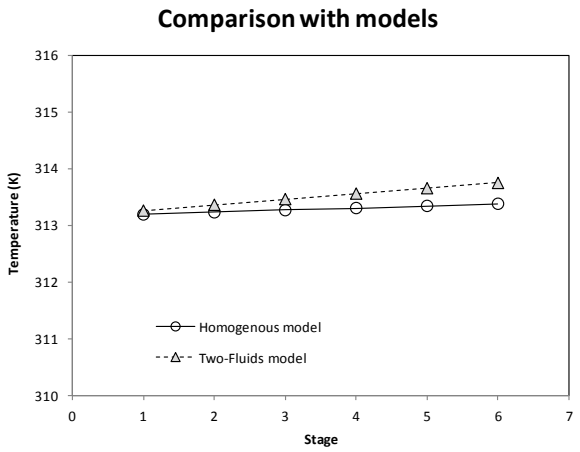

Figure 2 Comparison between the two models

The discrepancy between the two curves can be explained by the fact that with the two-fluid model, the temperature rise of gas during the compression depends on the gas temperature at the inlet of a stage - cf equation (23) - while the temperature elevation of liquid depends only on the pressure gain (cf equation (19). With the homogeneous model – cf equation (17), the average temperature elevation of the mixture is based on the temperature of the mixture at the inlet of the stage which is quite different than the temperature of gas. Therefore, the reference of the temperature at the inlet of the stage is not equal for the two models.

With the two-fluid model, it is possible to introduce a thermal kinetic of the heat exchange by taking into account the residence time of a particle through the stage. In that case the heat exchange is not completed and can be represented by the heat quantity actually exchange between gas and liquid, with the introduction of the partial coefficient θ.

$$Q_{gas/liq} = \theta \rho_{gas} q_{gas} c_{Pgas} \left(T_{f2} - T_{gas2} \right) \quad (28)$$

$$Q_{liq/gas} = \theta \rho_{liq} q_{liq} c_{Pliq} \left(T_{f2} - T_{liq2} \right) \quad (29)$$

The two terms represents the heat flux left by gas and the heat flux received by liquid respectively during the time needed for a particle to travel through the stage. Assuming a non-slippage condition between gas and liquid, the coefficient θ represents the ratio heat flux by conduction through a given number of bubbles divided by the total heat quantity of the volume of gas. Finally the coefficient is assessed using the equation given below:

$$\theta = \frac{3}{R_b^2} \left(\frac{\lambda_g}{\rho_g Cp_g} \right) \left(\frac{LS}{q_t} \right) \quad (30)$$

In (30), L and S represent the axial length and the cross area of the compression cell respectively, q_t the total flow rate, R_b the bubble radius, λ_g, ρ_g, Cp_g , the thermal conductivity, the specific gravity and the heat capacity of the used gas (i.e. diffusivity coefficient). In the case of a slippage condition between gas and liquid, the heat transfer considered could be a forced convection exchange in a dense mixture.

RESULTS AND COMPARISON

The two models have been used separately and are compared with the results performed by OneSubsea with a multistage multiphase pump (MPP) operated with actual conditions.

In this section, the results have been computed stage by stage using an in-house software introducing an adequate two-phase efficiency and a pressure gain multiplier coefficient depending on GVF and on the pressure at the inlet of the stage. Thus, as the conditions change at the inlet of each stage, the pressure gain and the efficiency in two-phase mixtures are computed from the performances of each stage in single-phase using the two multiplier coefficients.

The results presented in Figure 3 are obtained with the homogeneous model. The figure gives the global computed results in function of the experimental data for several values of GVF within the range [0 % - 90 %].

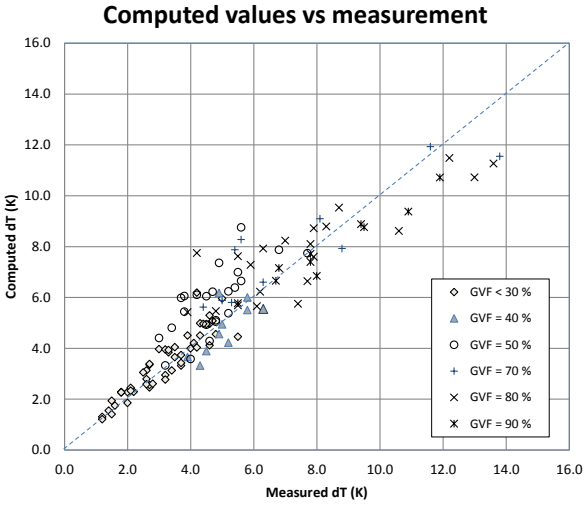

Figure 3 Comparison between the results from the homogeneous model and the experimental data

In the same manner, the figure 4 presents the results using the two-fluid model with a completed heat transfer between the gas and liquid.

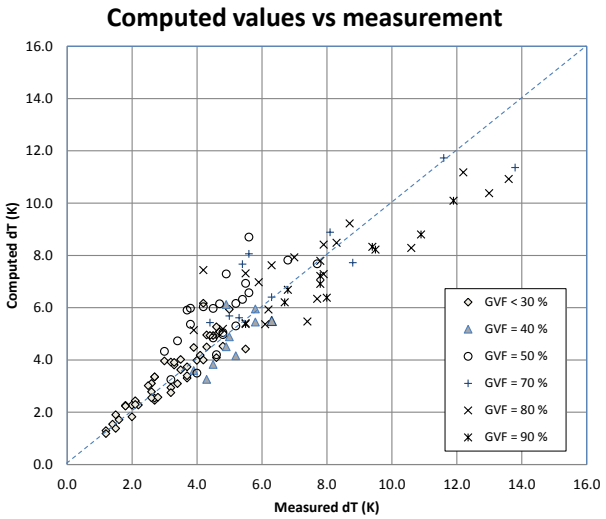

Figure 4 Comparison between the two-fluids model and the experimental data

From the figures 3 and 4, the figures 5 and 6 present the relative error of the global temperature rise between the inlet and the outlet of the pump, using the homogeneous model and the two-fluid model respectively.

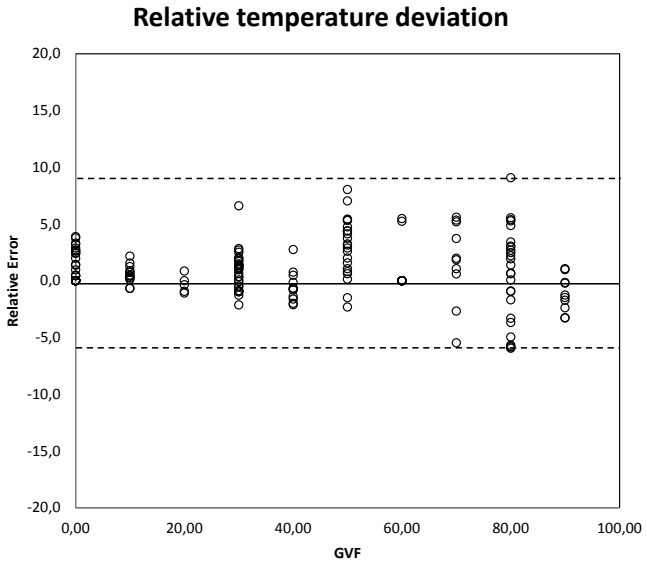

Figure 5 Relative errors with the homogeneous model

Globally, the results exhibit an increasing relative deviation from -5% to +10% when GVF increases from 50 % up to 80%. The use of the two-phase efficacy within the considered range of GVF explains partly this results. Another reason lies in possible errors of some measurements as the actual flow is not steady state.

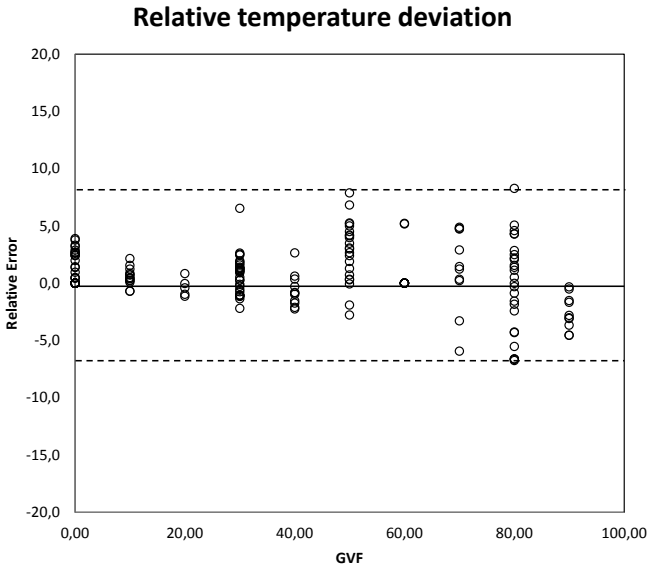

Figure 6 Relative errors with the two-fluids model

The results of the figure 6 using the two-phase model are quite similar to the results given on the figure 5 with the homogeneous model. The trends are very close to each other with increasing values in a range of GVF comprised between 50 % and 80 %.

CONCLUSION

The need of more powerful rotodynamic multiphase pumps for subsea applications in petroleum domains leads IFP Energies nouvelles and OneSubsea to design new technologies of pumps adapted to the operating conditions of a given field, especially for viscous fluids. The development of physical thermal models is needed to assess the temperature rise through each stage of an MPP.

Two models are detailed and discussed in the present paper. The first model concerns the compression of an homogeneous mixture of gas and liquid modifying the enthalpy of the mixture. The second one deals with a two-fluid model. The latter consists in the compression of each phase including a heat transfer between gas and liquid by conduction. The two developed models depend on the several parameters such as the pressure gain and the efficiency in two-phase flows. The used equations lead to results and trends very close to experimental data supplied by OneSubsea from tests performed with a multistage MPP operated with water and air. The accuracy of the model for the assessment of the global temperature rise through the whole pump is comprised within a range [-5 % ; 10 %]. More precisely, the relative error increases significantly in a range of Gas Volume Fraction (GVF) comprised between 50 % and 80 %.

The use of the homogeneous model is more simple than the second one. Nevertheless, the two-fluids model has an advantage compared with the homogeneous model by being capable of assessing the temperature of each phase at the outlet of the stages of the pump. Thus, the variations of gas flow rate

as well as the variation of liquid viscosity due to the effect of temperature rises could be predicted with a fine accuracy.

REFERENCES

[1] Lakshminarayana B., Fluid Dynamics and Heat Tranfer of Turbomachinery, *Wiley-Interscience Publication*, ISBN 0-471-85546-4, 1996.

[2] Wilson D.G. and Korakianitis T, The Design of High-Efficiency Turbomachinery and Gas Turbines – Second Edition, *Prentice Hall,* ISBN 0 -13 -312000-7, 1998.

[3] Wilson D.G., Analytical Models and Experimental Studies of Centrifugal Pump Performance in Two-Phase Flow, *EPRI report NP-677,* 1979.

[4] Gülich J.F., Centrifugal Pumps – Second Edition, *Springer,* ISBN 978-3-642-12823-3, 2010.

[5] El Hajem M., Vilagines R., Champagne J.Y. and Morel R., Measurement of Bubbly flows inside an axial Pump – A Feasibility Study, *HEFAT 2003*, Paper number HM2.

[6] Furuya O., An analytical Model for Prediction of Two-phase (Noncondensable) Flow Pump Performance, *Transaction of the ASME, Journal of Fluids Engineering,* March 1985, Vol 107, pp 139-147.

COMPARATIVE EXPERIMENTAL STUDY OF AIR-WATER VERTICAL ANNULAR FLOW THROUGH EXPANSION AND CONTRACTION SECTIONS

Anupriya .S and Jayanti .S[#]
[#]Author for correspondence
Department of Chemical Engineering,
Indian Institute of Technology, Madras,
Chennai,36,
INDIA,
E-mail: sjayanti@iitm.ac.in

ABSTRACT

Annular flow through a contraction or an expansion presents an interesting contrast; the different inertias of the three fields will generate different responses to the sudden deceleration or acceleration associated with expansion or contraction. In the present study, we report on the pressure profile measurements along the pipe wall as fully developed annular flow passes through the pipe expansion or pipe contraction. Experiments have been conducted through a vertical diverging or converging pipe section or through an abrupt transition with diameter ratios of 1.3 and 1.5. The pressure profiles show the response is characterized strongly by pressure recovery in the expansion. In the contraction, the pressure drop is accentuated by the pressure change associated with flow acceleration. Pressure loss coefficients for both the cases have been determined by extrapolating from measured upstream and downstream pressure profiles. It is found that the contraction loss coefficient is higher than the expansion loss coefficient for identical expansion/ contraction ratios. In cases of gradual area change, at high liquid flow rates, a strong vena contracta formation is found to occur in the expansion leading to a higher loss coefficient than for the contraction.

INTRODUCTION

Gas-liquid two phase flow through a vertical circular pipe occurs widely in many industrial equipment such as steam generators, reboilers, oil-gas transfer lines and other heat transfer equipments. While single-phase flows are well-understood for a number of complicated flow situations, two-phase flow in even simple geometries is largely ill-understood. Even in the case of two-phase flow through a vertical pipe, where the flow can be considered to be axi-symmetric, the flow is strongly affected by the thermophysical properties of the two fluids, their phasic flow rates, orientation of the pipe, dimensions of the pipe such as the diameter and the length of flow development, the way the two fluids are introduced in the pipe, etc. Depending on these and other factors, the gas and the liquid arrange themselves into a number of flow patterns [Collier, 1981]. Annular flow is one such flow pattern which offers the simplicity of being axi-symmetric and in apparent steady disposition of the phases. It is arguably the most studied and the best understood of the flow patterns [Hewitt and Hall-Taylor, 1970] although research into its nature is continuing with more and more sophisticated instruments [Lawrence et al., 2000]. At high gas flow rates, typically high enough to carry away liquid droplets sheared off the liquid film, annular flow becomes established in which part of the liquid phase flows along the wall in the form of a thin film which is dragged upwards by the gas phase while the rest flows in the form of fine entrained droplets in the gas core.

NOMENCLATURE

DP	[Pa]	Dynamic pressure
K	[-]	Loss Coefficient
U	[m/s]	Velocity
g	[m/s^2]	Gravitational acceleration
h	[m]	Loss head
f	[-]	Darcy friction factor
d	[m]	Smaller diameter
D	[m]	Larger diameter
Special characters		
ρ	[kg/m^3]	Density
Subscripts		
eq		Equivalent
avg		Average
f		Frictional loss
m		Minor loss
e		Expansion
c		Contraction
$core$		Gas core
$extr$		Extrapolation
acc		Acceleration

The dynamics of vertical upward annular flow have been described initially in terms of two-phase, two-field formulations involving droplet-laden gas core and liquid film; such models have been successfully used to predict dryout in tubes and rod bundles [Hewitt and Govan, 1990]. These have been extended to include droplets as a separate field leading to two-phase, three-fluid formulations which have been used to study dryout and post-dryout heat transfer in tubes and rod bundles [Jayanti and Valette, 2004; Jayanti and Valette, 2005]. Thus, quantitative models are available to describe the rate of

heat, mass and momentum exchange between these fields in fully developed and developing annular flow in straight tubes.

The presence of geometrical singularities in the flow field may affect the flow behavior of two phase as well as single phase flow and brings additional pressure drop associated with it. An insight into the pressure variation in single phase flow can be gained through computational fluid dynamics (CFD) simulations in which the velocity and pressure variations within the flow domain of interest are obtained by solving the governing Navier-Stokes equations numerically. CFD simulations are now well-established for the analysis of flow-related phenomena. Results obtained using the commercial CFD software, ANSYS-FLUENT, for the pressure variation in the case of a sudden expansion and a sudden contraction are shown in Figures 1a and 1b, respectively. In both cases, the Reynolds number based on the mean flow velocity and the diameter in the smaller pipe section was maintained at 100000 and the diameter ratio was 2.0. In the case of sudden expansion, the fluid decelerates as it goes into the larger diameter pipe leading to a substantial pressure recovery in the immediate downstream region; the flow becomes fully developed after several diameters downstream. During this process, a part of its kinetic energy is dissipated due to the formation of vena contracta resulting in an overall pressure loss, which is usually expressed in terms of a loss coefficient, K, which is defined as the ratio of pressure loss to the dynamic head in the pipe with smaller cross-sectional area. The loss coefficient for the case of sudden expansion is roughly given by

$$K_e = \left[1-\left(d/D\right)^2\right]^2 \qquad (1)$$

where d and D are the diameters of the smaller (upstream) and the larger (downstream) pipes, respectively.

In the sudden contraction case, the flow from the larger pipe accelerates as it enters the smaller one leading to a substantial reduction in the pressure associated with the change in the kinetic head. The computed pressure variation in this case is shown in Figure 1b. The nature of the flow is such that a small vena contracta is formed at the transition leading to pressure losses. An empirical correlation for contraction loss coefficient is given by

$$K_c = 0.42\left[1-\left(d/D\right)^2\right] \qquad (2)$$

One can see from equations (1) and (2) that the loss coefficient of contraction is less than half of that of expansion for the same diameter ratio. This is confirmed by the present CFD simulations which show a loss coefficients of 0.46 and 0.21 for the expansion and the contraction cases, respectively. It is expected that the loss coefficients would be lower when the area change is gradual.

The potential response of gas-liquid vertical annular flow across gradual expansion and contraction sections is shown schematically in Figure 2 in which the liquid film is shown in an exaggerated way for emphasis. The high gas speeds that are typical of annular flow and the consequent entrainment of droplets complicate the flow behavior in two-phase flow through pipe transitions. In the scenario of gradual expansion shown in Figure 2a, the gas core with a major fraction of the liquid flowing in the form of entrained droplets enters the larger diameter section and immediately experiences a flow deceleration. In the immediate downstream of expansion a fluctuating liquid film can occur [Anupriya and Jayanti, 2014]. The slowed down gas with a lesser fraction of entrained liquid develops eventually into the annular flow with a thicker liquid film.

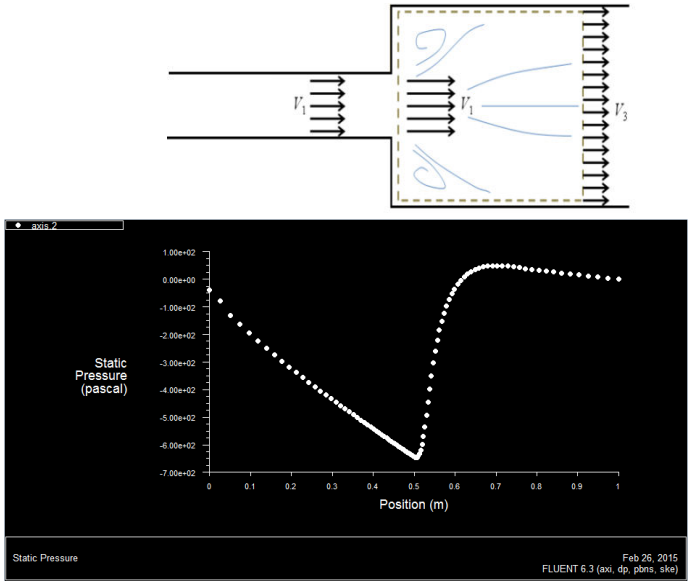

(a)

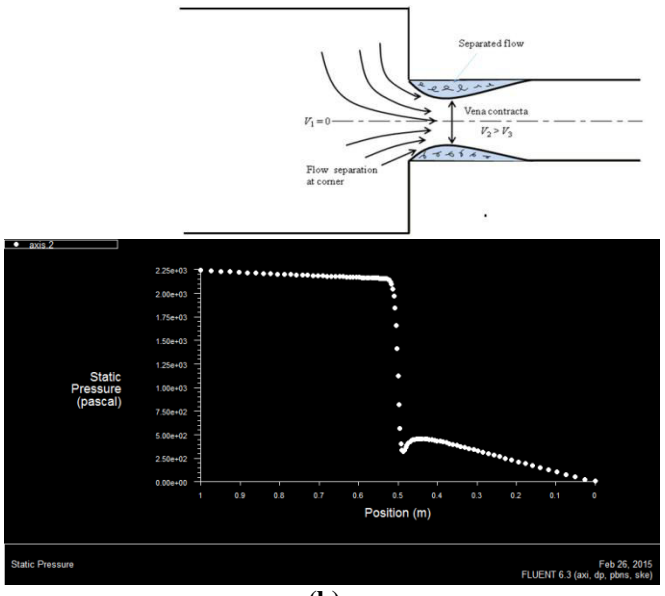

(b)

Figure 1. Calculated pressure variation along the centre-line in turbulent pipe through (a) a sudden expansion, and (b) a sudden contraction. Results have obtained using the commercial CFD software ANSYS-FLUENT.

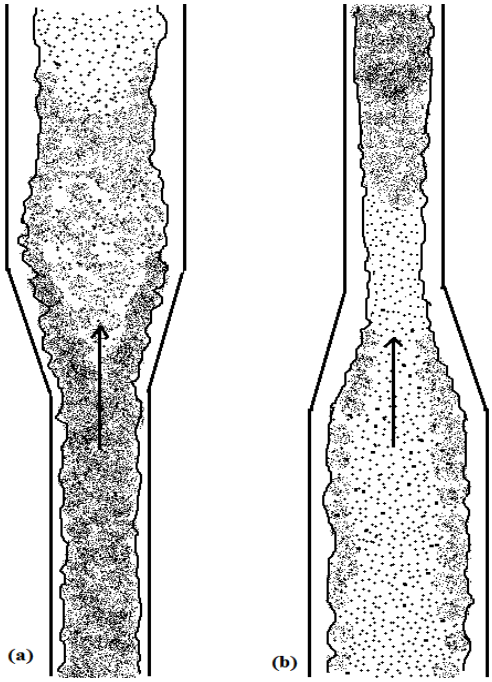

Figure 2. Response of gas-liquid vertical annular flow across (a) gradual expansion and (b) gradual contraction

In the case of gradual contraction, the gas core with less entrained droplets and a thicker liquid film approaches the contracting section. The blockage at the contraction leads to the inertial deposition of some of the large droplets which would otherwise have remained entrained. This leads to further thickening of the liquid film in the transition region. The excess liquid will eventually get entrained in the downstream section leading eventually to a fully developed annular flow. These conclusions are broadly in agreement with the results obtained by the application of the one-dimensional developing annular flow model of Kishore and Jayanti (2004). These special effects attributable to the presence of the liquid film may lead to higher pressure losses in contraction.

Despite their practical relevance, the cases of gradual expansion and contraction has not attracted much attention after the early studies of Chisholm & Sutherland (1961), McGee (1961), Lottes (1962) and Jansen & Kervinen (1964). The case of plate blockage in two phase flow has been studied by Tapucu et al. (1989); they reported finding liquid-rich, weak recirculation zone in the upstream section and high-void, strong recirculation zone in the downstream section. The pressure drop in contraction in various two phase flow regimes has been studied experimentally in the air-water system by Schmidt & Friedel (1996). The case of bubbly flow through a sudden expansion has been studied with respect to void fraction distribution, bubble size and velocities by Aloui & Souhar (1996, 1997). Higher turbulent intensity and void fraction in the immediate vicinity of a sudden expansion has been reported by Ahmed et al. (2007, 2008). An interesting observation of the disappearance of vena contracta at high liquid mass flux and gas quality in the case of contraction has been reported by Chen et al. (2009). In contrast, at very low gas quality, a phenomenon of 'liquid like vena contracta' has been observed by them accompanied by a detectable drop in the pressure change. Comparison of abrupt expansion and contraction pressure losses in mini channels has been explained using homogenous and separated models (Abdelall et al, 2004). A detailed comparison on abrupt and gradual contraction and expansion at various flow regimes in horizontal pipes has been reported by Kourakos et al. (2009). A theoretical study on pressure loss in abrupt area transitions of different diameter ratios has been reported by Roul and Dash (2011). Pressure drop across contraction has been redefined by Padilla et al. (2013) in terms of perturbation effects up and down streams, acceleration drop and frictional effects due to singularity. In a recent study (Anupriya and Jayanti, 2014) reported measurements of pressure loss coefficient in sudden and gradual expansions in vertical annular flow. The objective of the present work is to analyze the comparative effect of abrupt and gradual expansion and contraction sections in gas-liquid vertical annular flow to complement with the earlier study. A careful analysis of the response of expansion and contraction can be beneficial in understanding the dynamic processes that happen in annular flow.

EXPERIMENTAL SET-UP AND TEST PROGRAM

The experimental set-up for the pressure profile measurement in the diverging and converging sections consists of two vertical straight tubes with diameter ratios 1.3 and 1.5 with diameter combinations of 0.038 m/ 0.050 m and 0.0254 m/ 0.038 m. The flow system loop used for the present study is similar to the loop used by Anupriya and Jayanti (2014) and is shown in Figure 3. Each pipe combination has the cross section change either abruptly or gradually with half-included angle of either 15˚ or 8˚. Air was introduced axially to the vertical tube from an air compressor and water was introduced through a porous device. Such a set-up ensures the entry of water as a film all around the tube wall and air which causes this film to move upward. The air flow rate was measured using an orifice meter while the water flow rate was measured by a bank of three rotameters connected parallelly.

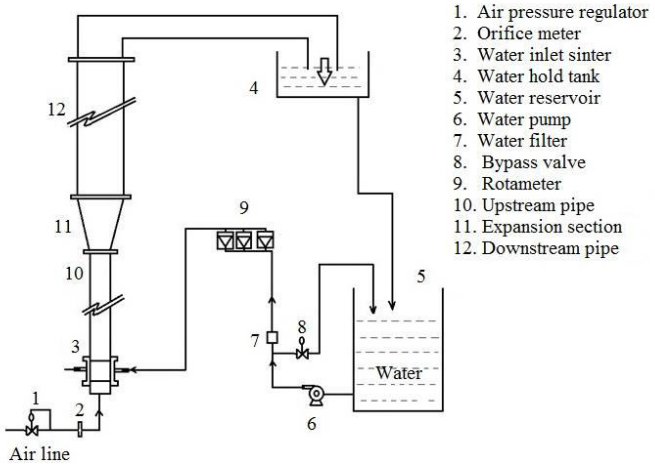

Figure 3. Schematic diagram of the air-water flow loop.

The air flow rate was maintained to ensure the annular flow regime at upstream and downstream section of the singularity and a development length of 2 m was provided to make sure the full development of flow before and after the transition section. The co-current air and water annular flow is collected in an open tank from which the water is recirculated. Six pressure taps were provided in the upstream section and 12 in the downstream section to measure the pressure profile. In case of gradual expansion/ contraction, one tapping for the 15^{o} transition and two tappings for the 8^{o} transition were located in the transition section itself. Experiments have been conducted in different combinations of air and water flow rate. In order to ensure annular flow, the air flow rate was varied in the range of 80 to 170 m^3/h while the water flow rate was varied in the range of 0 to 400 litre/h (LPH). Repeatability in experimental data was verified by conducting experiments under constant water flow with increasing air flow as well as under constant air flow with increasing water flow.

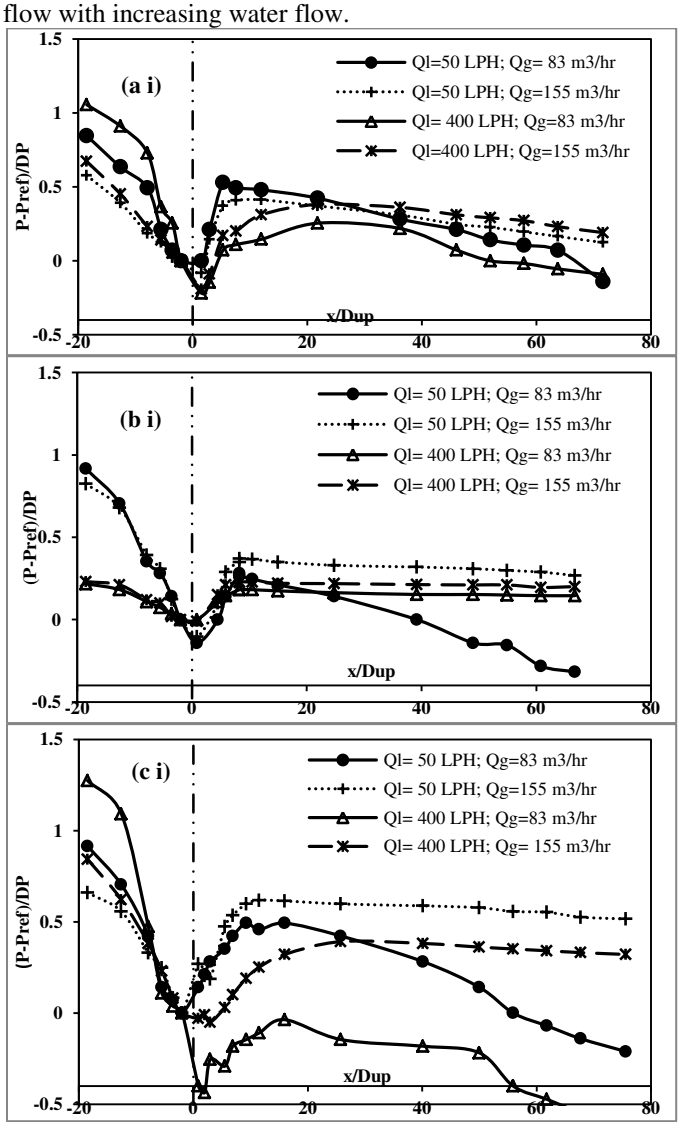

Figure 4. Variation of pressure drop across the diverging section with diameter ratio 1.5 (a i) sudden expansion, (b i) gradual expansion with half included angle 15˚and (c i) gradual expansion with half included angle 8˚

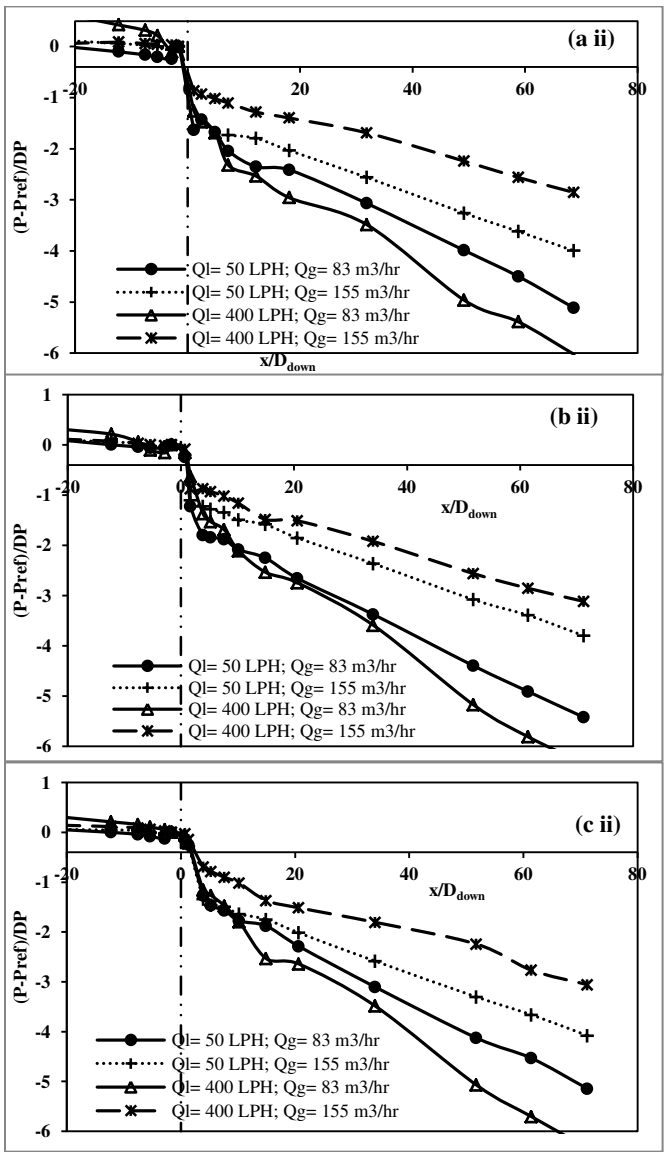

Figure 5. Variation of pressure drop across the converging section with diameter ratio 1.5 (a ii) sudden expansion, (b ii) gradual expansion with half included angle 15˚and (c ii) gradual expansion with half included angle 8˚

Typical variation of the measured pressure profiles in expansion and contraction are plotted in Figures 4 and 5, respectively, for four cases. Here, the pressure term has been non-dimensionalized using upstream superficial dynamic pressure corresponding to that of the gas core:

$$DP = \tfrac{1}{2}\rho_{core} u_{core}^{\ 2} \qquad (3)$$

The pressure variations in the sudden expansion case are qualitatively similar to those for single phase flow (Figure 1). However, there are noticeable effects of the liquid flow rate. In case of high gas flow rates, smooth pressure recovery has been observed. In case of low gas flow rates, the pressure recovery is sluggish, which has also been observed for high water flow rates. In the case of flow through the contraction, more pressure drop is observed in high liquid and low gas flow rates. This

may be explained as follows. As the gas core approaches the converging section, some droplets get deposited by inertial impaction. In the downstream section, the thick film gets entrained by the higher gas velocity. But in the case of low gas flow rates, the entrainment rate is not high enough and the film stays thick for a longer length causing higher pressure drop.

The irreversible pressure loss across the transition has been determined through extrapolation, as has been done previously by Chalfi and Gaiaasiaan (2007) and Anupriya and Jayanti (2014). This has been non-dimensionalized using the dynamic head as below:

For expansion, $\Delta p_{mixing} = K_e \left(\frac{1}{2} \rho_{core} u_{core}^2 \right)_{upstream}$ (4)

For contraction, $\Delta p_{mixing} = K_c \left(\frac{1}{2} \rho_{core} u_{core}^2 \right)_{downstream}$ (5)

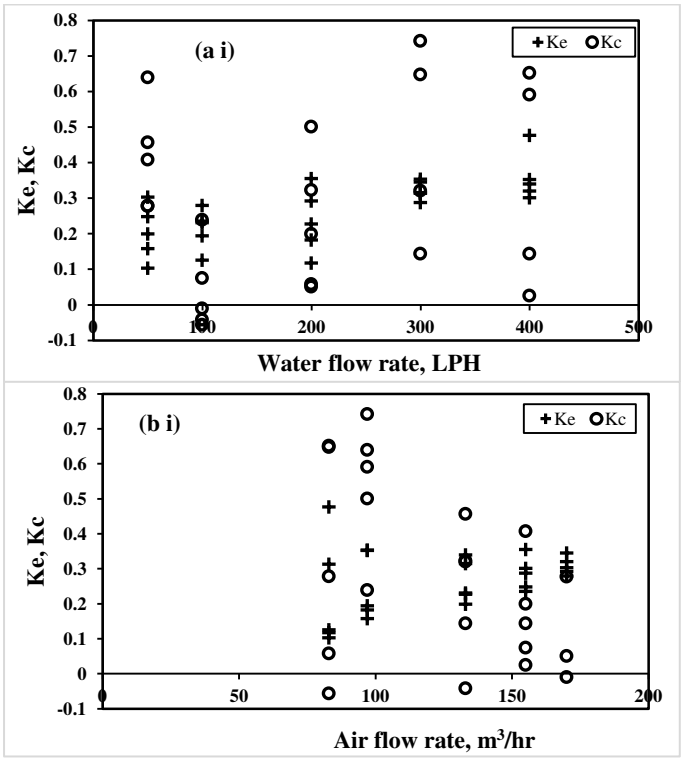

Figure 6. Ke-Kc comparison of sudden area change at (a i) constant water flow rate and (b i) constant air flow rate

The results obtained for a number of cases are summarized in Figure 6,7 and 8. In general, the loss coefficient due to contraction seems to be higher than that due to expansion. As the liquid flow rate increases, the contraction loss coefficient is found to be increasing due to the effect of more lump formation. But as gas flow rate increases, it decreases because the accelerated gas can pull the liquid lumps easily. In the case of expansion, the loss coefficient increases slightly as liquid and gas flow rate increase. In the gradual area transition cases, K_e increases with air and water flow rates, as observed in sudden expansion. But K_c is higher at lower air and water flow rates and is decreasing with the increase in flow rates.

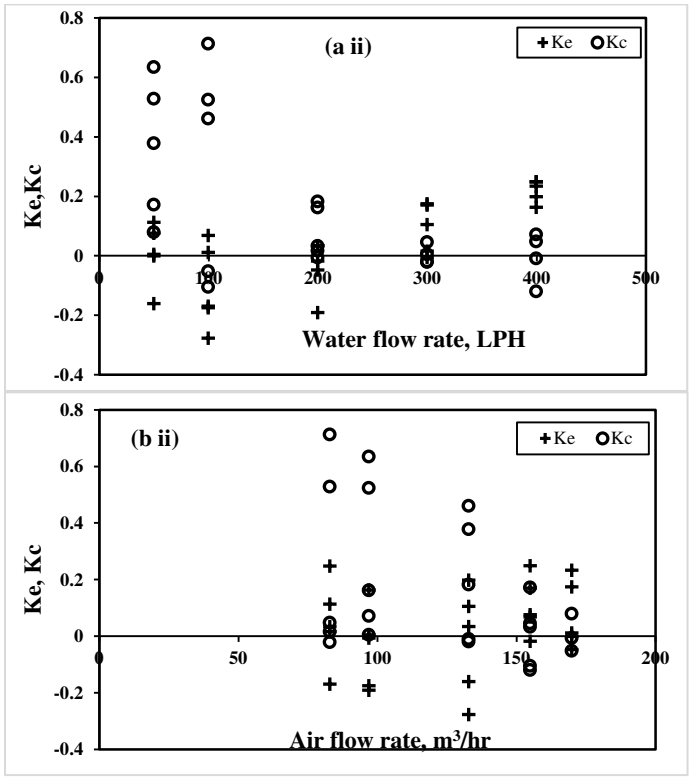

Figure 7. Ke-Kc comparison for area change at a half included angle of 15˚ at (a ii) constant water flow rate and (b ii) constant air flow rate

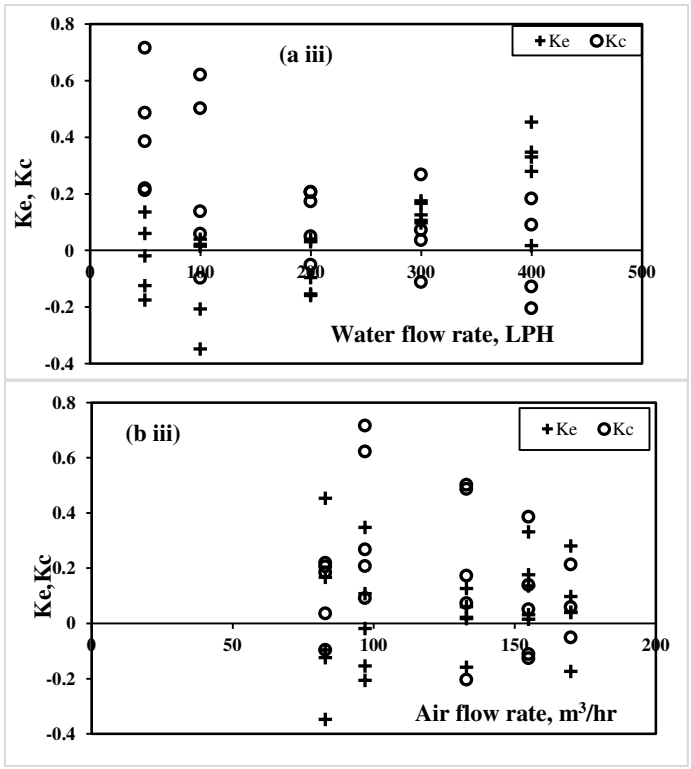

Figure 8. K_e-K_c comparison for area change at a half included angle of 8˚ at (a iii) constant water flow rate and (b iii) constant air flow rate

CONCLUSION

Comparative study of expansion and contraction loss coefficients in vertical gas-liquid annular flow using experimental data for both gradual and sudden area transitions has been carried out experimentally. Unlike in the case of sudden area change in single phase flow, two phase annular flow results show higher contraction losses in many flow rate combinations. In sudden transition case, the higher K_c value has been found for higher liquid flow rates and lower gas flow rates. This is an indication of heavy liquid lump formation at sudden contraction due to blockage effect.

REFERENCES

[1.] Abdelall, F.F., Hahn, G., Ghiaasiaan, S.M., Abdel-Khalik, S.I., Jeter, S.M., Yoda, M., Sadowski, D.L.,. Pressure drop caused by abrupt flow area changes in small channels. *Exp. Therm. Fluid Sci*. 29, 2005,425–434.

[2.] Ahmed, W.H., Ching, C.Y., Shoukri, M.,. Development of two-phase flow downstream of a horizontal sudden expansion. *Int. J. Heat Fluid Flow* 29, 2008,194-206.

[3.] Ahmed, W.H., Ching, C.Y., Shoukri, M.,. Pressure recovery of two-phase flow across sudden expansion. *Int.J.Multiphase flow*, 33, 2007, 575-594.

[4.] Aloui, F., Souhar, M., Experimental study of two-phase bubbly flow in a flat duct symmetric sudden expansion part 1; visualization, pressure and void fraction. *Int.J.Multiphase flow*, 22, 4, 1996, pp- 651-665.

[5.] Aloui, F., Souhar, M., Experimental study of two-phase bubbly flow in a flat duct symmetric sudden expansion part 2; liquid and bubble velocities, bubble sizes. *Int.J.Multiphase flow*, 22, 5, 1996, pp-849-861.

[6.] Anupriya, S., Jayanti, S., Experimental and modelling studies of vertical annular flow through diverging section. *Int.J.Multiphase flow*., 67, 2014, pp- 180-190.

[7.] Chalfi, T.Y., Ghiaasiaan, S.M. ,. Pressure drop caused by flow area changes in capillaries under low flow conditions.*Int. J. Multiphase Flow* 34 (1), 2008, 2-12.

[8.] Chisholm, D., Sutherland, L.A.,. Prediction of pressure gradients in pipeline systems during two-phase flow. *Proc.I.Mech.E.* 184, 1969, 24-32.

[9.] Collier, J.G., Convective boiling and condensation , Mc Graw-Hill, NY, USA, 1981.

[10.] Hewitt, G.F., Hall-Taylor, N.S.,. Annular Two-Phase Flow. Pergamon Press, Oxford, UK. 1970

[11.] Hewitt, G.F., Govan,A.H.,. Phenomenological modelling of non-equilibrium flows with phase change. *Int. J. Heat Mass Transf*. 33, 1990, 229–242

[12.] Ing Youn Chen, Chin Yung Tseng, Yur Tsai Lin, Chichuan Wang., Two phase flow pressure change subject to sudden contraction in smaller rectangular channels, *Int.J.Multiphase flow*, 35, 2009, 297-306.

[13.] Jansen, E., Kervinen, J.A.,. Two-phase pressure drop across contraction and expansion, steam-water mixture at 600–1400 psia.*Report GEAP-4622*, General Electric Company, San Jose, California, 1964

[14.] Jayanti, S., Valette, M., 2004. Prediction of dry out and post-dry out heat transfer at high pressures using a one-dimensional three-fluid model. *Int. J. Heat Mass Transf*.47, 4895-4910.

[15.] Jayanti, S., Valette, M., 2005. Calculation of dry out and post-dry out heat transfer in rod bundles using a three-fluid model. *Int. J. Heat Mass Transf*.48(9), 1825-1839.

[16.] Kourakos, V.G., Rambaud, P., Chabane, S., Buchlin, J.M., Modeling of pressure drop in two-phase flow in singular geometries. Paper No. MN-30, *6th International Symposium on Multiphase Flow, Heat Mass Transfer and Energy Conversion* Xi'an, China, 2009

[17.] Kishore, B.N., Jayanti, S.,. A multidimensional model for annular gas–liquid flow. *Chem. Eng. Sci.* 59, 2004,3577 – 3589.

[18.] Lawrence, C. J., Hawkes, N.J., Hewitt, G.F., Studies of wispy-annular flow using transient pressure gradient and optical instruments. *Int.J. Multiphase Flow*. 26,10, 2000, pp 1565-1582.

[19.] Lottes, P.A.,. Expansion losses in two-phase flow. *Nucl. Sci. Eng.* 9, 26–31,1961

[20.] Mc Gee, J. W., Two phase flow through abrupt expansion and contraction, PhD Thesis, University of North Carolina at Raleigh USA, 1966.

[21.] Padilla, M., Revillin, R., Bonjour, J., Two phase flow of HFO-1234yt, R-134a & R-410A in sudden contraction: Visualization, pressure drop measurements and new prediction method. *Exp. Therm. & Fluid sci.*, 47, 2013, 186-205.

[22.] Roul, K., Dash, S.,. Two-phase pressure drop caused by sudden flow area contraction/expansion in small circular pipes. *Int. J. Numer. Meth. Fluid*. 66, 2011, 1420–1446

[23.] Schmidt, J., Friedel, L., Two phase pressure drop across sudden contraction in duct areas. Int.J.Multiphase flow, 23, 2, 1997, 283-299.

[24.] Tapucu, A., Teyssedou, A., Troche, N,. Merilo, M,. Pressure losses caused by area changes in a single channel flow under two-phase flow. *Int.J.Multiphase flow,* 15, 1, 1989, pp 51-64